Article

Not peer-reviewed version

Sequence Stratigraphical Applications of Organic Microfacies Analysis in the Devonian Rocks, Faghur Basin, Western Desert, Egypt

Walid Ahmed Makled , Ali Ismail Al-Juboury , Asmaa Kamel , Ali Ismail Elshorbagy , Mohamed Mahmoud El Garhy , Nagham Omar , Thomas Gentzis * , Nasir Alarifi , Fathy Abdalla *

Posted Date: 25 March 2026

doi: 10.20944/preprints202603.1900.v1

Keywords: chitinous sheets; tunicate spicules; stratigraphical correlation; sequence stratigraphy; Devonian evolution

 doi:10.20944/preprints202603.1900.v1

Article

Sequence Stratigraphical Applications of Organic Microfacies Analysis in the Devonian Rocks, Faghur Basin, Western Desert, Egypt

Walid Ahmed Makled [1], Ali Ismail Al-Juboury [2], Asmaa Kamel [3], Ali Ismail Elshorbagy [4], Mohamed Mahmoud El Garhy [4], Nagham Omar [5], Thomas Gentzis [6,*], Nasir Alarifi [7] and Fathy Abdalla [7,*]

[1] Exploration Department, Egyptian Petroleum Research Institute (EPRI), 1 Ahmed El Zomor St. Nasr City, Cairo 11727, Egypt
[2] Petroleum Engineering Department, College of Engineering, Al-Kitab University, Kirkuk, 36015, Iraq
[3] Geology Department, Faculty of Science, Damnhour University, Egypt
[4] Al-Azhar University, Faculty of Science, Geology Department, P.O. Box 11884, Cairo, Egypt
[5] Institut für Geowissenschaften, Geologie, University of Bonn, Nussallee 8, 53115, Bonn, Germany
[6] Core Laboratories, Petroleum Services, 6316 Windfern Road, Houston, TX 77040, USA
[7] Geology and Geophysics Department, College of Science, King Saud University, Riyadh 11451, Saudi Arabia
* Correspondence: thomas.gentzis@corelab.com (T.G.); fabdalla@ksu.edu.sa (F.A.)

Abstract

The Paleozoic rocks of Egypt's Western Desert remain under limited exploration. Complex subsurface structures create stratigraphic challenges that hinder petroleum exploration. Organic microfacies analysis offers a precise and effective tool to address these challenges and enhance our understanding of environmental changes. The Faghur-1X well penetrated the Devonian Zeitoun Formation, yielding numerous successful core recoveries. Seven of these cores were analyzed to delineate lithological and stratigraphical variations. Three distinct organic microfacies types were identified within the studied section. These organic microfacies reveal significant paleoenvironmental shifts that represent key correlative events within the Devonian. These include liptinite-dominated-medium organic density distal facies (A) (cores 19-A, 18-B, 17-A); vitrinite-dominated-high organic density proximal facies (B) (cores 14-A, 20-A/Band 20-C); ironstone rich and low organic density condensed section/distal facies (cores 18-A, 16-A, 15-A, 15-B). These organic facies exhibit unique characteristics resulting from the interaction of organic matter with the rock matrix and environmental processes. These unique characteristics facilitate intra-basinal stratigraphic correlation. While commonly applied to hydrocarbon source rock evaluation, this study investigates the stratigraphic significance of organic microfacies for resolving subsurface geological problems.

Keywords: chitinous sheets; tunicate spicules; stratigraphical correlation; sequence stratigraphy; Devonian evolution

1. Introduction

The Paleozoic rocks in the subsurface of the Western Desert of Egypt offer promising opportunities for petroleum exploration [1,2]. The Devonian rocks comprise an important division of the Paleozoic rocks that are frequently encountered during deep subsurface petroleum exploration in the Faghur Basin. However, many problems challenged the continuous development in the fields that mostly have resulted from the stratigraphic classification and correlation difficulties [2]. In the last decade, the Devonian rocks in the Faghur Basin were subjected to detailed research that explored the paleoenvironmental settings and sequence stratigraphic classifications that depended on the palynofacies and well logs as well as the biostratigraphic zonation [3,4]. The study of palynofacies

 doi:10.20944/preprints202603.1900.v1

offers an accurate tool for stratigraphic correlation and classification that is based on the organic matter to interpret and track the environmental changes [5]. However, important information is lost during the preparation of palynological samples, most importantly the rock fabric and groups of other microfossils.

Organic microfacies analysis is another tool that explores the organic content in the rock sample. Unlike palynofacies, it keeps the rock fabric and other microfossil groups. According to the definition of Stasiuk et al. [6], organic microfacies refers to the textural and spatial relationships observed under a microscope between the various components of a rock. These components include individual macerals (microscopically identifiable constituents of organic matter), kerogen-rich layers, the remains of microscopic fossils (both organic and inorganic), micro-ichnofossils (microscopic traces of biological activity), and the surrounding mineral matter (the host rock). The most important aspect of organic microfacies is the study of the textural relationships between the rock matrix and organic matter. Although their study pertained to the depositional environmental controls on maceral type, Stasiuk et al. [6] focused on the application of the organic facies in the evaluation of hydrocarbon source rocks and cyclic changes in the sedimentary systems. In the present study, a similar approach is suggested to develop the stratigraphic application of organic microfacies. Organic microfacies represent the interplay of continuous biological evolution and dynamic processes of the environment. This gives organic microfacies the merits of diversity and individuality in time and space, which is a basic requirement in stratigraphic tools that can be used for correlation purposes.

The Devonian rocks are subjected to intensive studies for their source rock potentiality in the Middle East and North Africa [3,4,7–10]. In the present study, core samples are available from the Faghur-1X well, which penetrated a thick Devonian section. This well was drilled for exploration purposes in 1958. Twenty-seven cores were extracted during the drilling and their lithological variations were described (Faghur-1X lithology well log, 1958). This well provides the opportunity to describe the organic microfacies in seven of these cores. The organic microfacies are described and correlated to other locations in the Faghur basin, North Africa and Gondwana regions based on their similarity. This approach aims to develop the use of organic microfacies as a stratigraphic tool.

2. Geological Settings

In the Faghur-1 well (Figure 1), the Devonian section reaches 1051 meters (3450 ft) and is primarily composed of clastics, with black shale intercalations up to 234 meters (800 ft) thick (Figure 2). These Devonian rocks, belonging to the Zeitoun Formation, are exclusively and completely preserved within Faghur-1X. The sandstones are predominantly fine-grained, occasionally grading to silt-sized particles. The black shale is gray to dark gray and silty (Figures 1 and 2). Devonian geological data in northwest Egypt is primarily derived from twelve wells described by Klitzsch [11], supplemented by limited outcrops in the Western Desert's southwest, assigned to the Wadi Malik Formation [12). Subsurface Devonian strata are predominantly clastic, consisting of light-colored, porous sandstones and siltstones with interbedded fossiliferous black shales reaching 150–200 meters thick [11]. These clastics suggest a partially marine environment, transitioning southward to increased continental influence, represented by open to shallow marine sediments with deltaic and fluvial intercalations. Further south and east, this formation has been progressively eroded and is absent beneath Carboniferous strata [13] (Figure 3). The recent studies dealt with the Devonian rocks in the Buchis-1X (Devonian rock thickness 435 ft) and the Phiops-1X (Devonian rock thickness 100 ft) wells northeast of the Faghur-1X well, where the thickness of the section is significantly reduced [14]. The thickness in the southwest of the Faghur-1X in the Sifa-1X well reaches 2470 ft [4]. The significant variation in the thickness of Paleozoic rocks in the Faghour Basin presents a major exploration challenge. This problem manifests as difficulties in subsurface correlation and the interpretation of seismic line connectivity, leading to a high-risk environment for field development in these areas. The reason for thickness variations is attributed to structural elements, which required further investigations. Devonian rocks in both the Faghur Basin (Egypt) and the Cyrenaica Platform (Libya) are primarily siliciclastic, comprising sandstones and siltstones with shale intercalations [3,14,15].

 doi:10.20944/preprints202603.1900.v1

These deposits thicken northward and southward towards the Jebel Akhdar uplift [16], and were primarily deposited in shallow marine, deltaic, and fluvial environments [16].

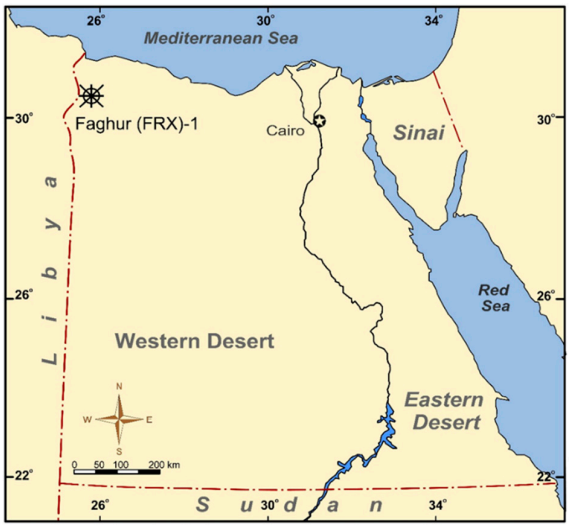

Figure 1. Location map of the Faghur-1 well in the Western Desert of Egypt.

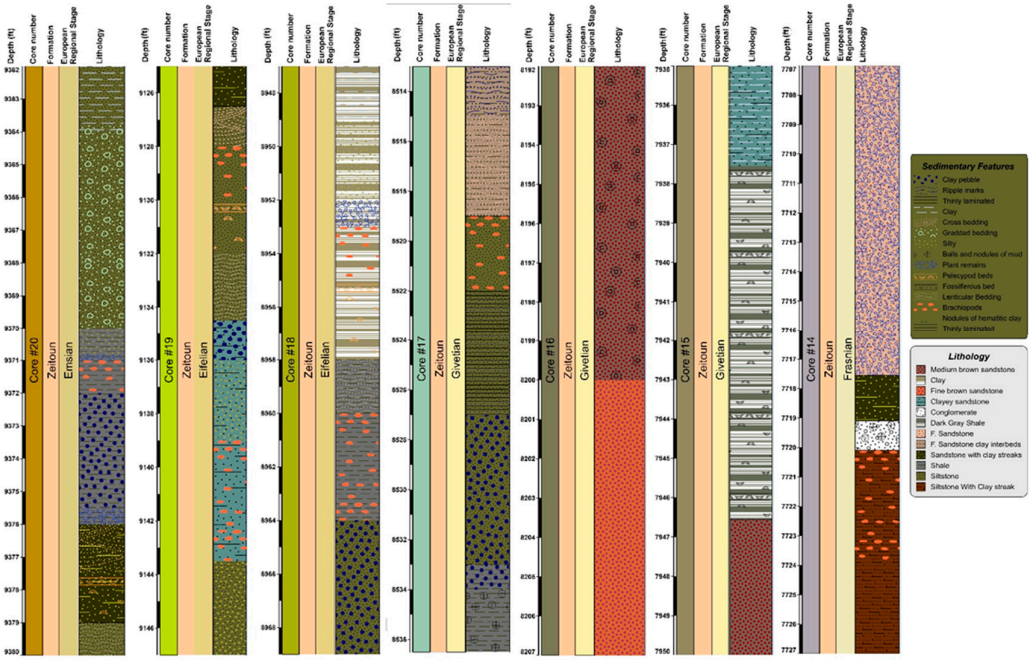

Figure 2. Lithological variations and core descriptions.

 doi:10.20944/preprints202603.1900.v1

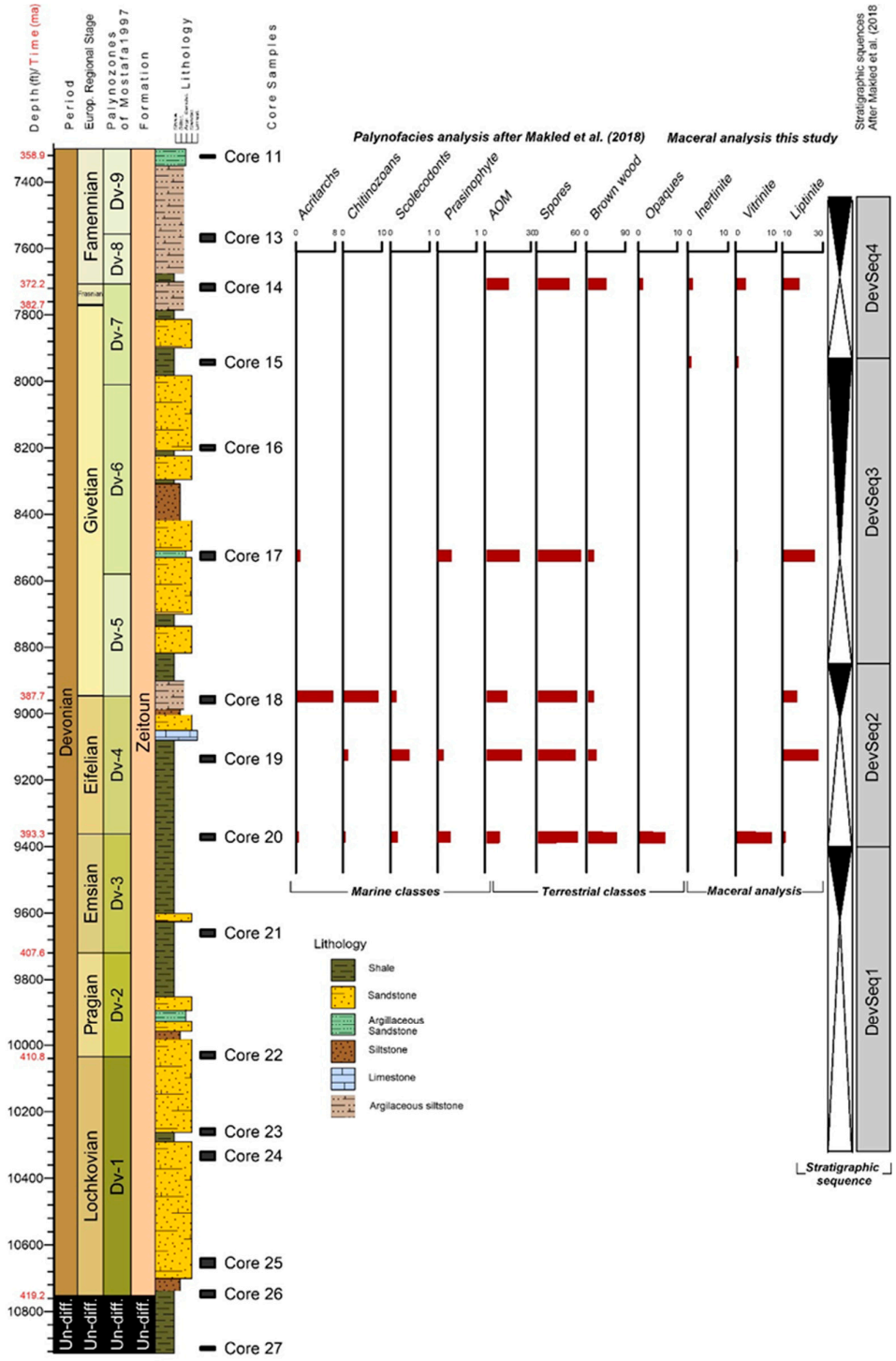

Figure 3. Stratigraphic column of the Faghur-1 well. Biostratigraphy is after Mostafa et al. [28]. The distribution of the palynofacies classes and stratigraphic sequences is after Makled et al. [3]. The maceral analysis is accomplished in the present study.

 doi:10.20944/preprints202603.1900.v1

3. Material and Methods

3.1. Organic Petrography and Statistical Analysis

The drilling plan in the Faghur-1 well provided the best opportunity to study the interactions between depositional environments and evolution of organic matter in the Devonian and Paleozoic rocks. The drilling plan included 27 core sections that cover the total depth of the well at 10925 ft. The cores are distributed over the total drilled thickness at rate of about 1.2 cores for every 1000 ft in the upper 6000 ft interval (7 cores in 6046 ft). This interval covers the Cenozoic and Mesozoic rocks. Afterward, the rate changed to 3.9 cores every 1000 ft (19 cores in 4925 ft). This interval confines the Paleozoic rocks with consideration of one core (core number 12) having junk in the hole. The Paleozoic section starts at the top of probable Permian strata at a depth of 6040 ft that is determined to be near to the top of core number 8 (6046-6074 ft). The Carboniferous starts at 6270 ft and includes only one core (core number 9). The Devonian interval begins at 6840 ft and contains 15 cores starting from core number 10 (6887-6928 ft) to core number 25 (10640-10668 ft). Undifferentiated Lower Paleozoic interval starts at 10665 ft to the total depth of 10925 ft and includes two cores (26 and 27) (Figures 2 and 3). The total thickness of cores reaches 346 ft that is equal to about 0.07% of the total Paleozoic interval and 0.09% in Devonian interval alone (Figures 2 and 3). Eleven samples were collected from 7 cores starting from core number 14 (7707 to 7727 ft) to core number 20 (9362-9380 ft) (Figures 2 and 3). The samples are represented by discs of about 1 to 2 cm thickness.

The samples were cut by an electric machine diamond saw to cubic grains of about 1 cm and placed in the solidification molds (4.2 cm in diameter). The arrangement considers that the final polished surface should be normal to their bedding and lamination directions as well as parallel to the bedding plan. Sample preparation and polishing followed established procedures [17,18]. Specifically, samples were initially embedded in epoxy resin. A low-viscosity epoxy resin was used to ensure thorough penetration. After curing, the embedded samples were sectioned and then polished to a mirror finish using progressively finer abrasive grits on a polishing wheel. Polished pellets were prepared to examine the relationship between organic matter and the surrounding mineral matrix. The detailed petrographic characterization was performed using a Leica DM4 microscopic system optimized for reflected light. The maceral composition and nomenclature adhered to international standards, including ASTM D2799 [19], ASTM D7708-23a [20], and the International Committee for Coal and Organic Petrology guidelines for vitrinite [21], inertinite [22], and liptinite [23] classification. The results of organic petrography are categorized into distinct organic facies through statistical cluster analysis using Ward's method [24].

3.2. Palynofacies and Biostratigraphic Analyses

To isolate organic matter, a two-step acid digestion is performed. First, 10% HCl was used to dissolve the carbonates, followed by 40% HF to dissolve the silicate framework [25–27]. The resulting residue was filtered through a 10 μm Nylon mesh then neutralized and concentrated. Strew mounts were examined under transmitted white and incident blue light to identify fluorescing palynofacies and organic microfossils. The biostratigraphic zonation of Devonian rocks in Faghur-1X well was performed by Mustafa [28] and El Shamma et al. [29] based on palynomorphs. There biozonation divisions discriminate the section into nine palynozones from Dv-1 (Lochkovian) to Dv-9 (Famennian) (Figure 3). The palynofacies categories were classified and quantified using the Tyson [30] scheme to interpret paleoenvironmental trends and sedimentary cyclicity. The palynofacies analysis was conducted and studied by [3] and classified by cluster analysis into palynofacies types. Same authors constructed a sequence stratigraphic scheme including 4 sequences (DevSeq1 in the lower part to DevSeq3 in the upper part) (Figure 3). This scheme was used also in the present study to indicate the stratigraphic position of the organic microfacies in the sequence stratigraphic framework.

 doi:10.20944/preprints202603.1900.v1

3.3. Supervised Machine Learning and Maceral Quantification

White incident light was utilized for the identification and labeling of non-fluorescent macerals, such as high-reflectance inertinite and medium-reflectance vitrinite. On the other hand, fluorescence incident light was employed to detect the liptinite group (e.g., sporinite) based on its distinct auto-fluorescence properties. This multi-modal approach addresses the complex and heterogeneous nature of organic matter, which often limits the effectiveness of fixed-size window identification methods [31]. For every analyzed field of view, white light and fluorescence photomicrographs were captured, coregistered, and merged into multi-channel stacks using the Fiji (ImageJ) distribution [32] (Figure 4). This process ensured that each pixel was characterized by both reflectance and fluorescence attributes. This facilitates precise spatial identification and significantly reduces the subjectivity and discrepancies inherent in manual petrographic evaluations [33]. The method of maceral quantification followed the method detailed in Makled et al. (submitted).

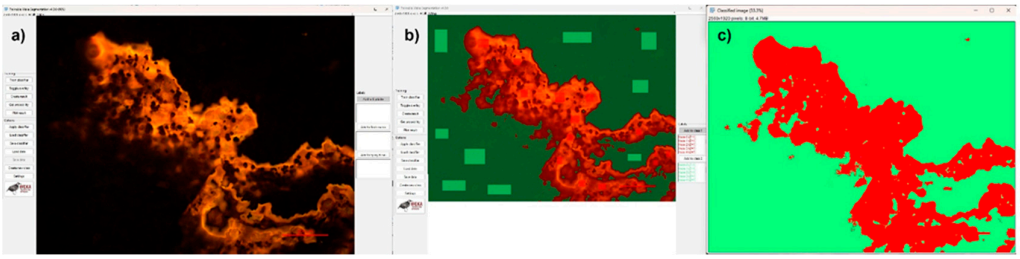

Figure 4. Sequential stages of the automated maceral identification workflow using Fiji ImageJ Trainable Weka Segmentation (TWS). (A) Original multi-modal photomicrograph showing the raw distribution of organic and inorganic phases in fluorescence mode. (B) Training phase where representative areas are labeled to train the Random Forest classifier, reducing subjective bias. (C) Final segmented output where pixels are categorized by class, enabling the precise quantification of total organic density (TOD).

The automated segmentation of organic components was performed using the Trainable Weka Segmentation (TWS) plugin, employing a Random Forest classifier. This algorithm was selected due to its proven robustness against overfitting and its efficiency in handling high-dimensional feature sets in petrographic thin sections compared to traditional neural networks [34]. The classifier uses a feature space comprising 80 attributes, including hue, saturation, and brightness, alongside advanced texture and edge filters such as Sobel, hessian matrices, and membrane projections. The multiscale Gaussian features, ranging from sigma = 1.0 to 16.0 pixels, were integrated to account for the diverse morphology and size of maceral groups. The Random Forest model is configured with 100 iterations (I = 100) and a bag size of 100 (P = 100). This uses the ensemble learning principles outlined by Witten and Frank [35] to achieve stable and generalized classification.

The classification performance was evaluated using 10-fold stratified cross-validation. This method involved partitioning the labeled dataset into ten subsets. Each model was trained on nine subsets and tested on the remaining one in a rotating cycle. The reliability was quantified using correctly classified instances (%) and Kappa statistic to measure overall agreement. Moreover, the mean absolute error (MAE) and root mean squared error (RMSE) were used to assess the magnitude of prediction errors. The precision and recall were used to evaluate class-specific performance for vitrinite, inertinite, and liptinite.

The total organic density (pixel area %) was calculated as the cumulative area percentage of all organic macerals (Vitrinite + Liptinite + Inertinite) relative to the total area of the field of view.

$$Total\ organic\ density = \frac{\sum Pixels_{\ organic}}{\sum Pixels_{Total}}$$

This pixel-based quantification ensured a more objective and repeatable measurement compared to traditional manual point-counting methods.

 doi:10.20944/preprints202603.1900.v1

3.4. Total Organic Carbon (TOC)

The Organic Density derived from Random Forest segmentation was calibrated against LECO-derived TOC values to validate pixel-based spatial quantification. This cross-validation ensures that the microscopic heterogeneity captured by multi-modal imaging reflects the true carbon storage capacity of the lithofacies. The bulk geochemical validation was conducted using a LECO SC32 Analyzer of 5 samples. The Pulverized samples were decarbonatized with 10% HCl at 60^{0}C to isolate the organic fraction. The residues were then subjected to high-temperature induction combustion (>1300^{0}C) under pure oxygen. The resulting CO_2 was measured via an integrated Non-Dispersive Infrared (NDIR) detector. This mass-based TOC measurement provided a calibration baseline for the pixel-based Organic Density derived from the digital petrography workflow.

4. Results

4.1. Cores Lithological Variations

Core 20 extends between depths of 9380 and 9362 ft (thickness of 18 ft). This core is dated to the Emsian, confining Palynozone Dv-3 during the sea level rise of sequence DevSeq2 (Figures 2 and 3) [3,28,29]. The lithological variations exhibit a general upward coarsening trend. The lower 4 ft of the core consists of lenticular siltstone at the base, which grades upwards into fine sandstone containing clay streaks and thin beds of shells. This is succeeded by a 14-ft thick section that begins with a shale bed rich in plant remains. This shale grades into a unit characterized by clay pebbles and brachiopods, eventually transitioning into a siltstone showing graded bedding and shale rich in plant remains (Figure 2). Core 19 ranges between 9125 and 9147 ft (thickness of 22 ft). This core is of Eifelian age and is limited by Palynozone Dev-4 within the maximum flooding surface of sequence DevSeq2 (Figures 2 and 3) [3,28,29]. The core shows a general coarsening upward stacking pattern. The lower 10-ft interval is composed of silty fine sandstone at its base, grading into clayey medium sandstone rich in brachiopod fossils, which becomes silty at the top (Figures 2 and 3). The succeeding interval begins with a shale bed containing clay pebbles and grades into fine to medium siltstone with lenticular bedding. The core top part encloses fossiliferous fine to medium sandstone featuring shale streaks (Figures 2 and 3).

Core 18 is positioned between 8947 and 8969 ft (thickness of 22 ft). Its age is Givetian based on Palynozone Dev-5 during the sea level fall of sequence SeqDev 2 (Figures 2 and 3) [3,28,29]. Unlike the previous cores, this interval displays a fining upward stacking pattern. The lower 8 ft is distinguished by a transition from siltstone with clay pebbles in the lower part to silty shale that contains brachiopod fossils in the upper part (Figure 2). The remaining 13-ft upper section is composed of siltstone that grades into dark gray shale with silty and clayey intercalations (Figure 2). Core 17 extends from 8513 to 8536.5 ft (thickness of 23.5 ft). The age is also Givetian, associated with Palynozone Dev-6 at the maximum flooding surface of sequence SeqDev-3 (Figures 2 and 3) [3,28,29]. The core is characterized by a coarsening upward stacking of facies. The lower portion is composed of shale, which grades into thinly laminated coarse siltstone. The middle and upper parts of the core consist of fine sandstone with clay streaks, mud nodules, and brachiopods (Figures 2 and 3). Core 16 extends between 8192 and 8207 ft (thickness of 15 ft). It is also of Givetian age within Palynozone Dev-16 during the sea level fall of sequence SeqDev-3 (Figures 2 and 3). This core represents part of a significant interval of iron oxide-rich sediments. Lithology is primarily composed of two beds forming a coarsening upward pattern. The lower bed consists of fine brown sandstone, which changes upwardly to medium brown sandstone containing hematite nodules in hand specimens (Figsures 2 and 3). Core 15 is situated between 7950 and 7935 ft (thickness of 15 ft). This core is also of Givetian age within Palynozone Dev-7 during the sea level rise of sequence SeqDev-4 (Figures 2 and 3) [3,28,29]. The lower part of the core, below 7946.5 ft, is composed of ironstone that continues the coarsening upward trend observed in Core 16. However, the texture of the coated grains in this ironstone becomes generally finer in the upper section (Figsures 2 and 3). The upper part of the core consists of dark gray shale at the base, which grades into clayey sandstone at the top, further

 doi:10.20944/preprints202603.1900.v1

delineating a coarsening upward trend (Figures 2 and 3). Core 14 extends between 7707 and 7727 ft (thickness of 20 ft). This core is of Frasnian age within Palynozone Dev-7 at the maximum flooding surface of sequence SeqDev-4 (Figures 2 and 3) [3,28,29]. This interval exhibits two fining upward stacking patterns. The section from 7727 to 7720 ft is composed mainly of fossiliferous siltstone that grades into siltstone rich in brachiopods. The final section, from 7720 to 7707 ft, is composed of conglomerate at the base, which transitions into sandstone and fine sandstone containing plant remains at the top (Figures 2 and 3).

4.2. Organic Density

The reliability of organic matter quantification was assessed through stratified 10-fold cross-validation. The statistical summary (Tables 1 and 2, Figure 4) confirms a high degree of precision in the segmentation of the organic components. The Kappa statistic (0.9985-0.99) signifies a near-perfect agreement between the predicted classes and the reference labels, ensuring that the subsequent density calculations are highly representative. The mean absolute error (MAE 0.0003-0.02) and root mean square error (RMSE 0.0064-0.07) were exceptionally low. This indicates that the model's probability estimates are stable and that large classification errors are virtually absent. The Relative Absolute Error (RAE 2.6%-4.95%) and root relative squared error (RRSE 7.9%-15.1%) values further validate that the error is minimal even when compared to the variance of the underlying dataset.

Table 1. Detailed accuracy and error parameters of the segmentation model for samples 14-A, 18-B, and 19-A, illustrating the statistical validity of the pixel-based Organic Density quantification.

Stratified cross-validation (10 folds)	19-A sample	18-B sample	14-A sample
Correctly Classified Instances	140699 (99.9%)	97117(99.5%)	173181 (100%)
Incorrectly Classified Instances	4 (0.0028%)	527 (0.54%)	15(0.01%)
Kappa statistic	0.9985	0.99	0.9997
Mean absolute error	0.0003	0.02	0.003
Root mean squared error	0.0064	0.07	0.02
Relative absolute error	2.6172%	4.98%	1.7864%
Root relative squared error	7.9321%	15.1%	6.05%
Total Number of Instances	140703	97644	173196

Table 2. Lithological, organic characteristics and main fingerprint of the organic microfacies including the organic density in area percentage. The distribution of the palynofacies classes and stratigraphic sequences is after Makled et al. (2018). The maceral analysis is accomplished in the present study.

Organic microfacies	Depth (ft)	Total organic density	Liptinite	Vitrinite	Inertinite	Acritarchs	Chitinozoans	Scolecodonts	Prasinophyte	AOM	Spores	Translucent Phytoclasts	Non-translucent Phytoclasts	Lamination	Organic microfacies
14-A	7707	10.0	6.0	3.0	1.0	0.0	0.0	0.0	0.0	18.8	43.8	36.4	1.0	1	B
15-A	7942	6.0	4.4	0.9	0.7	0.0	0.0	0.0	0.0	0.0	0.0	0.0	0.0	0	C
15-B	7948	0.1	0.1	0.0	0.0	0.0	0.0	0.0	0.0	0.0	0.0	0.0	0.0	1	C
16-A	8203	0.0	0.0	0.0	0.0	0.0	0.0	0.0	0.0	0.0	0.0	0.0	0.0	0	C
17-A	8525	2.0	1.5	0.5	0.0	0.7	0.0	0.0	0.4	27.5	59.6	11.9	0.0	1	A
18-B	8948	1.1	0.8	0.3	0.0	7.6	9.6	0.1	0.0	17.5	53.7	11.6	0.0	0	A
18-A	8968	1.3	1.2	0.1	0.0	0.0	0.0	0.0	0.0	0.0	0.0	0.0	0.0	0	C
19-A	9125	7.9	7.9	0.0	0.0	0.0	1.2	0.5	0.2	29.4	52.2	16.6	0.0	0	A
20-C	9371	9.0	3.4	5.6	0.0	0.4	0.5	0.2	0.4	11.4	54.7	28.8	3.8	1	B
20-A/B	9374	11.1	0.0	11.1	0.0	0.0	0.0	0.0	0.0	10.6	25.8	56.4	7.2	1	B

 doi:10.20944/preprints202603.1900.v1

Precision metrics highlight the advantage of using a multi-modal machine learning approach. The absolute precision (1.000) achieved for the liptinite group supports the use of fluorescence incident light as a primary discriminator. Similarly, the high precision of vitrinite (0.991) ensures that organic density variations across the stratigraphic column are a true reflection of the organic abundances, with negligible interference from the inorganic mineral matrix.

The organic density distribution across the sampled depth interval (7707 to 9374 ft) exhibits a distinct bimodal pattern characterized by significant enrichment at the stratigraphic extremes and depletion in the mid-section (Figures 5 and 6). High organic concentrations were mostly found in samples 20-A/B at 9374 ft at the bottom of the studied section with a density of 11.1%, and in sample 14-A at 7707 ft with a density of 10.0% at the top. Other high-density samples include 20-C (9.0%) and 19-A (7.9) located near the base of the studied interval. A low-density zone was observed between approximately 7948 ft and 8968 ft. In this zone, the value dropped to a minimum of 0.0 in sample 16-A (8203 ft) and 0.1 in sample 15-B (7948 ft).

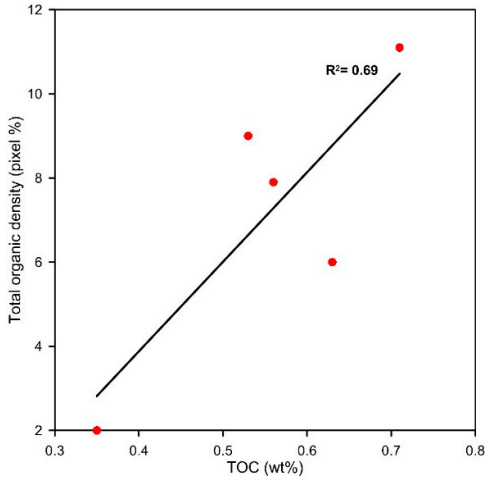

Figure 5. Cross-plot comparing the quantitative results of the Random Forest classification (Organic Density) with bulk induction combustion analysis (TOC). The R^2 value of 0.69 reflects the model's ability to accurately capture organic enrichment trends.

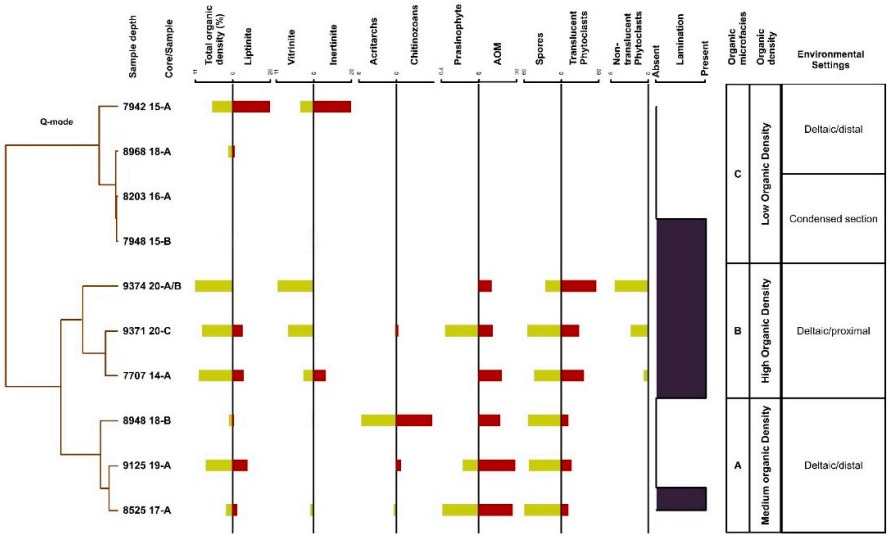

Figure 6. Dendrogram of the Q-mode cluster analysis performed on ten core samples showing the organic microfacies and total organic density in the studied core sample.

 doi:10.20944/preprints202603.1900.v1

The relationship between the petrographically derived organic density (pixel area %) and the geochemical total organic carbon (wt %) was evaluated by linear regression analysis. The resulting cross-plot yields a correlation coefficient of $R^2 = 0.7$ (Figure 5). This positive correlation demonstrates that the Random Forest classifier successfully captures the stratigraphic trends in organic enrichment. The statistical significance of this R^2 value confirms that the pixel-based segmentation of multi-modal micrographs (white light and fluorescence) is a reliable proxy for the bulk carbon content of the formation.

4.3. Organic Microfacies

The description of organic microfacies as the most comprehensive tool to characterize rock composition was studied systematically in the present study. The systematic items that were used to describe organic microfacies identified in the cores of the Faghur-1X well include the organic and inorganic matter, all types of microfossils and rock minerals as well as the rock fabric. Organic density was also introduced to describe the organic matter net accumulation and preservation in the rock matrix, an important characteristic element in organic microfacies. The target of this description was to understand the interactions between these different components. These interactions help establish the identity of organic microfacies stratigraphic fingerprints in sequence stratigraphic framework. Based on the cluster analysis, the samples were distinguished and classified into 3 organic microfacies based on the dendrogram of Q-mode (Figure 6).

Medium organic density-Liptinite dominant organic microfacies A: These organic microfacies include 3 core samples (19-A, 18-B and 17-A) (Figure 6). Sample 19-A was collected at a depth of 9125 ft from medium grained sandstone (Figure 2). The most abundant organic matter is the relatively thick dark brown chitinous sheets (Figures 7 and 8). These brown sheets are partially interconnected and crumpled beneath rock polished surfaces and many reach to 0.3 mm in length (Figure 7 (7-8) and Figure 8). Many sheets show wrinkles and bends within the leveled rock matrix (Figure 7 (5, 7-8)). In higher magnifications, the sheets show low reflectance and brown color in white light and strong dark yellow in blue light (Figure 7 (10-13)). They comprise the most abundant organic matter found in the sample (7.9%). There is no trace of cell structures on the surface of the sheets. The sheets are covered with a thin film of darker matter that doesn't fluoresce like the internal parts (Figure 7 (5-13)). The single sheet is composed of two layers that are separated by a thin surface that extend through the entire sheet (Figure 7 (9)). Other macerals detected include cutinite (Figure 7 (1 and 2)) and sporinite (Figure 7 (3 and 4)). In the palynofacies analysis spores (52.2%), Amorphous Organic Matter (AOM) (29.3%) and translucent phytoclasts (19.6%) were the dominant classes (Figure 3) [3]. Total organic density reached 7.9% (Table 2, Figures 4 and 5). There is no record of mineralic microfossils. The sample was composed of massive sandstone (Figure 8). The samples showed irregular and wrinkled sheets of brown chitinous matter that formed a wafer-like structure within the rock matrix (Figure 7 (5-13) and Figure 8).

 doi:10.20944/preprints202603.1900.v1

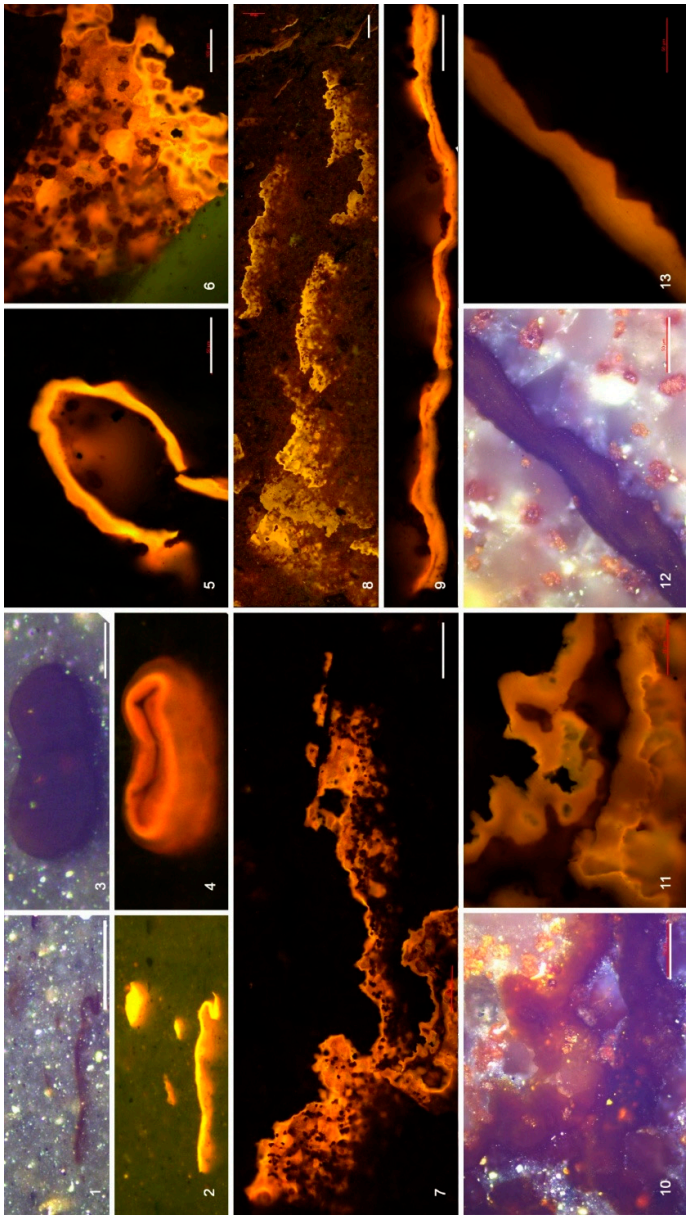

Figure 7. Organic microfacies (A) 19-A. 1-5, 6, 9-13 scale bar 50µm, 7, 8 scale bar 200µm. 1,2 Cutinite. 23, 4 sporinite. 5-13 chitinous sheets with distinctive brown color and orange fluorescence color. 1, 3, 10, 12 are in white incident light. 2, 4, 9, 11, 13 in blue incident light. 9 chitinous sheet with thin film that separates the sheet into two layers. 13 chitinous sheet with two layers.

Sample 18-B was collected at a depth of 8948 ft (Figure 2). These organic microfacies witnessed the highest diversity and abundance of marine organic matter including prasinophytes, acritarchs and chitinozoans in addition to diverse and abundant terrigenous organic matter, such as spores and plant woody tissues (Figure 9 (1-4, 22)). This organic matter is comprised of liptinite macerals such as alginite and sporinite (0.8%) as well as vitrinite (0.3%) (Table 2). The prasinophytes were abundant in these organic microfacies and were comprised of sacs of phycomata of Tasmanitids (Figure 9 (10, 16-18)) and Cymatiosphaerids (Figure 9 (14, 15)). Acritarchs were also abundant and diverse including acanthomorphs (Figure 9 (2, 4, 19) prismatomorphs (Figure 9 (5)) and Sphaeromorphitae accretions of multiple grains (Figure 9 (6-9)). Chitinozoans were also found in abundant numbers and mostly contain pyrite (Figure 9 (20, 21)). Spores were also abundant and diverse and were distinguished by their relatively large and spiny forms (Figure 9 (3, 4, 11)). Other terrigenous organic matter includes vitrinite (Figure 9 (22)) and cutinite (Figure 9 (12). The palynofacies analysis revealed

 doi:10.20944/preprints202603.1900.v1

a similar composition, whereby the acritarchs (7.5%), chitinozoans (9.5%) and scolecodonts (0.13%) dominated the marine palynomorphs (Figure 3). The spores (53.6%) were the dominant palynofacies class while the translucent phytoclasts reached 11.5% (Figure 3). The organic matter density was 1.1% (Table 2, Figures 3 and 6). There is no indication of other mineralic microfossils in these organic microfacies. The rock matrix was massive and the distribution of organic matter was sporadic (Figure 9).

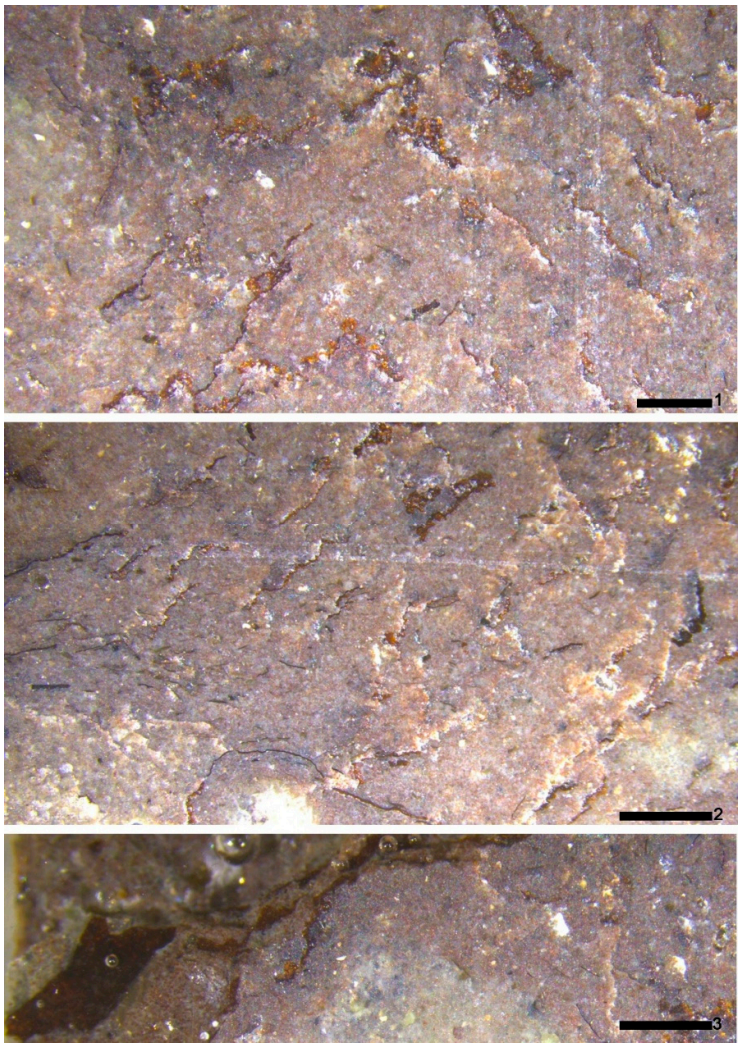

Figure 8. Rock section photomicrographs of the Organic microfacies (A) 19-A. 1, 2 scale bar 500μm. 3 scale bar 350μm. 1-3 thin lamination of the rock matrix with rock matrix.

 doi:10.20944/preprints202603.1900.v1

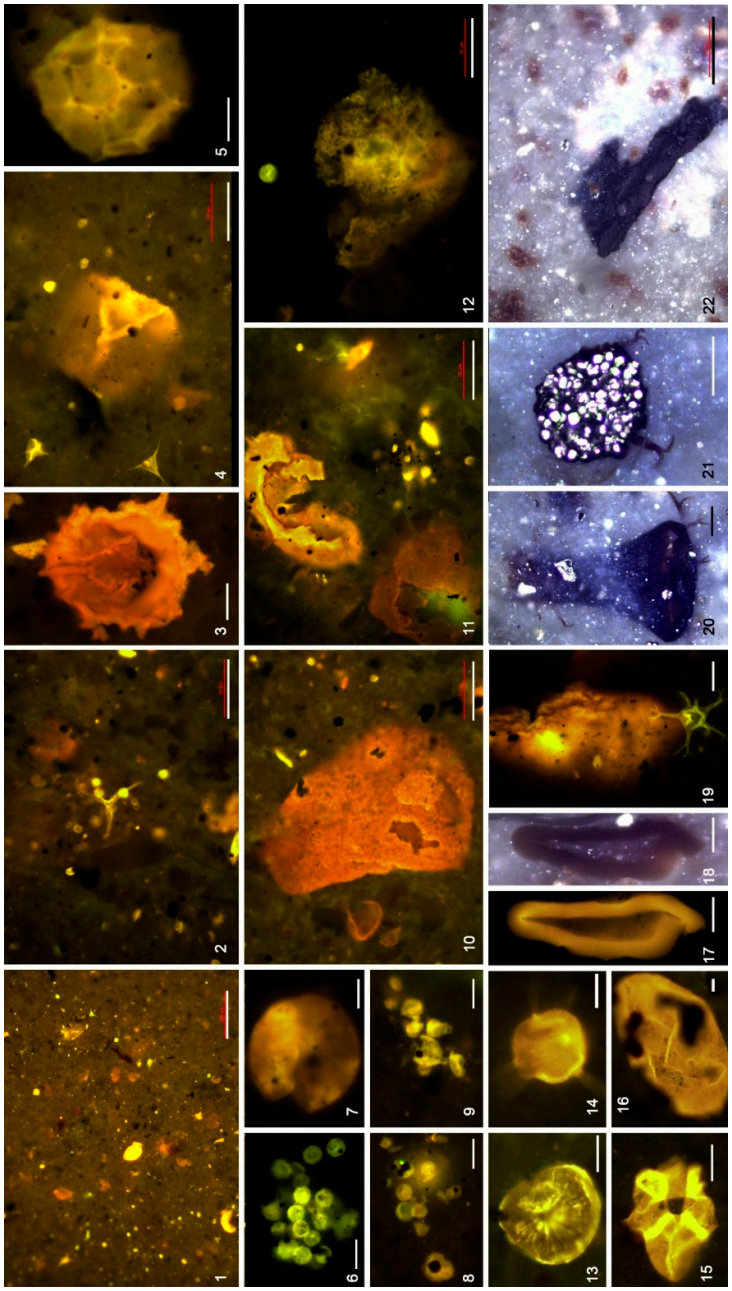

Figure 9. Organic microfacies (A) 18-B. 1-5, 11, 11, 12, 22 scale bar 50µm, 6-21 scale bar 10µm. 1, 2 Large field showing the distribution of organic matter. 3, 4, 11 Spores and acritarchs (acanthomorphs). 4, 19 Acritachs (acanthomorphs). 5 Prismatomorphs. 10, 16-18 Tasmanitids. 12 Cutinite. 14, 15 Cymatiosphaerids. 6-9 Sphaeromorphitae accretions of multiple grains. 20, 21 Chitinozoans. 22 Vitrinite. All photomicrographs are in blue incident light except 18, 20-22 are in white incident light.

Sample 17-A was collected at a depth of 8525 ft from the thinly laminated siltstone (Figure 2). The organic matter is like the 18-B organic microfacies and characterized by liptinite (1.5%) (alginite and sporinite) and vitrinite (0.5%) (Table 2, Figure 6). Alginite represented most of the marine organic matter and was composed mainly of acritarchs (Figure 10 (1-4)) and prasinophytes (Figure 10 (10-11)). The chitinous sheets were still present but changed in the texture and became more porous (Figure 10 (12-15)). The size of the alginite grains became smaller than that recorded in the sample 18-B organic microfacies (Figure 9). Sporinite was abundant but less diverse in these organic microfacies (Figure 10 (1-4)). Vitrinite became more abundant and larger in size (Figure 10 (5 and 6)). The palynofacies analysis revealed a similar distribution of the classes where the spores were most

 doi:10.20944/preprints202603.1900.v1

abundant (59.6%) and translucent phytoclasts were less dominant (11.8%) (Figure 3). The marine palynomorphs included acritarchs (0.6%) and prasinophytes (0.39%) (Figure 3). AOM (27.44%) was also abundant in organic microfacies (Figure 3). The organic matter density reached 2% (Table 2). These organic microfacies contained no mineralic microfossils. This sample showed weak lamination of the organic matter within rock matrix perpendicular to the bedding direction (Figure 10). In addition, the density of the organic matter was high in the rock section leveled parallel to the bedding (Figure 10). Vitrinite aligned with the spores and lamination of the rock matrix (Figure 10 (1, 5-8)).

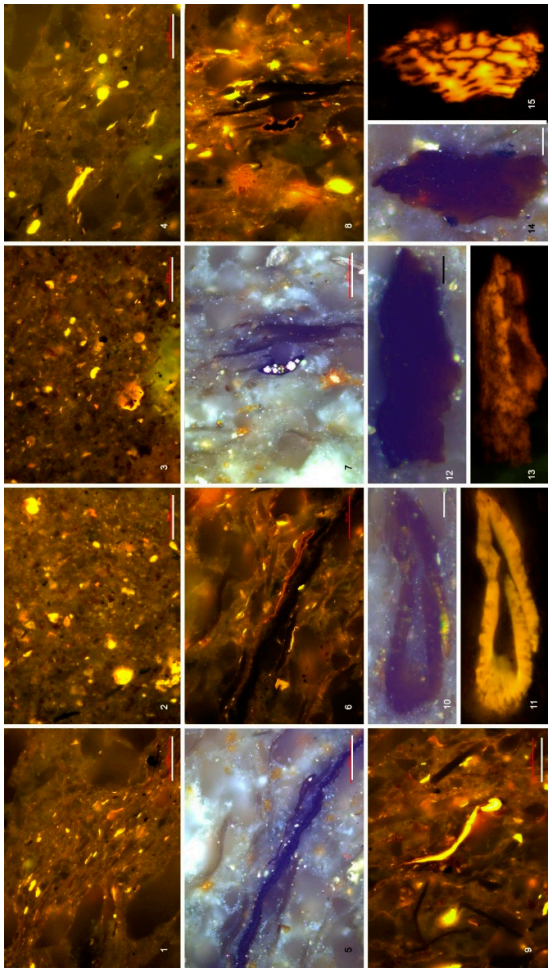

Figure 10. Organic microfacies (A) 17-A. 1-9 scale bar 50µm, 10-15 scale bar 10µm. 1-9 large fields show the distribution of organic matter that includes mostly acritarchs. 1, 5-8 Vitrinite and sporinite alignment with lamination of the rock matrix. 10-11 Prasinophytes. 12-15 chitinous sheets. All photomicrographs are in blue incident light except 5, 7, 10, 12, 14 are in white incident light.

High organic density-Vitrinite dominant organic microfacies B: These organic microfacies include three samples (20-A/B, 20-C and 14-A) (Table 2, Figure 6). Two samples (20-A/B) were collected at a depth of 9374 ft from the shale bed (Figure 2). The organic composition consisted of thin brown sheet-like particles (11.1%) (Figure 11 (1); Figure 12 (1-5)). These particles lacked internal structure and had a weak reflectance (Figure 12 (1-5)). They also lacked fluorescence in reflected blue light (Figure 12 (2 and 4)). These particles were identified as vitrinite based on the above optical properties (Figure 12 (1-5)). Each particle was composed of the multiple sheets of brown organic matter (thickness 5 µm, Figure 12 (5)) that occasionally merged on each other forming one grain. These particles were abundant in the rock matrix in different lengths forming continuous surfaces that extended throughout the full length of the rock fragments (Figure 12 (5)). Abundant sulfide minerals were observed surrounding these sheet-like particles. The density of the sulfide mineral increased at the

 doi:10.20944/preprints202603.1900.v1

rims and could be traced through the full length of particles. No other organic particles were observed in the rock samples (Table 2). However, the counting of concentrated organic matter in palynofacies analysis revealed the occurrence of other organic particles such as spores (25.8%), non-translucent (7.7%), and AOM (10.6%) with translucent brown phytoclast that reached up to 56.3% (Figure 3). The organic matter density was 11.1% (Table 2). No mineralic microfossils were observed in these microfacies. The rock contained abundant pyrite and was composed mainly of siltstone. The distinguishing features in sample 20-A/B organic microfacies included thin laminations that were clearly visible by the parallel arrangement of the sheet-like organic particles (Table 2, Figures 11 (1) and 12 (1-5)). The rock matrix was distinguished into layers that were separated by lamina of coarse grains. The particles reached 0.1 mm and they were uniform in size (Figure 11 (1) and Figure 12 (1-5)). Although the particles were distributed uniformly within each layer, their abundances were not equal between different layers (Figure 11 (1); Figure 12 (1-5)). Several levels of lamination couplets were observed in these organic microfacies including: 1) organic rich lamina and rock mineral lamina (Figure 12 (5)), 2) rhythmic increase of dense organic matter (Figure 12 (5)), and 3) coarse silt (light) and fine silt lamina (dark) (Figure 12 (1)).

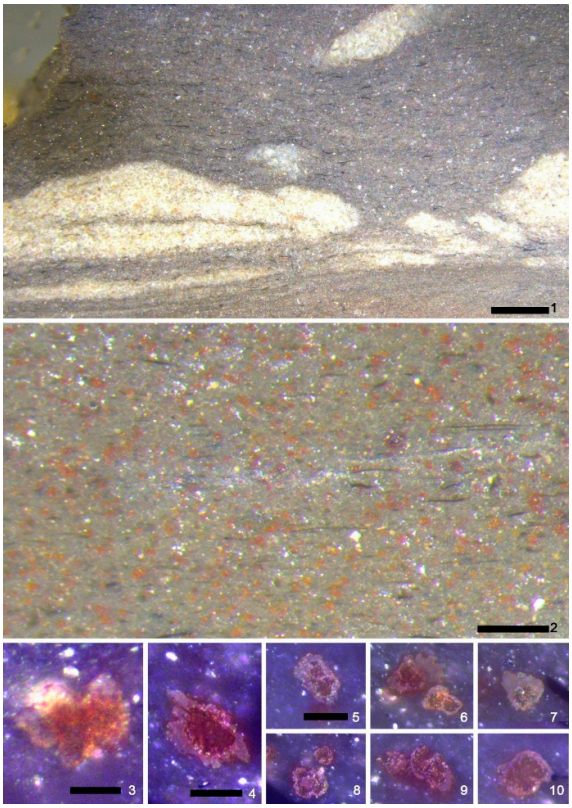

Figure 11. Rock section photomicrographs of the organic microfacies (B), samples 20 –A/B and 20-C. 1, 2 scale bar are 500 μm, 3-10 scale bar are 10 μm. 1 Thinly laminated plant remains in lathlike shape in Organic microfacies 20 –A/B. 2 Thinly laminated plant remains in lathlike shape in Organic microfacies 20 –C, orange dotes are tunicate spicules. 3-10 Tunicate spicules of different forms in Organic microfacies 20 –C.

 doi:10.20944/preprints202603.1900.v1

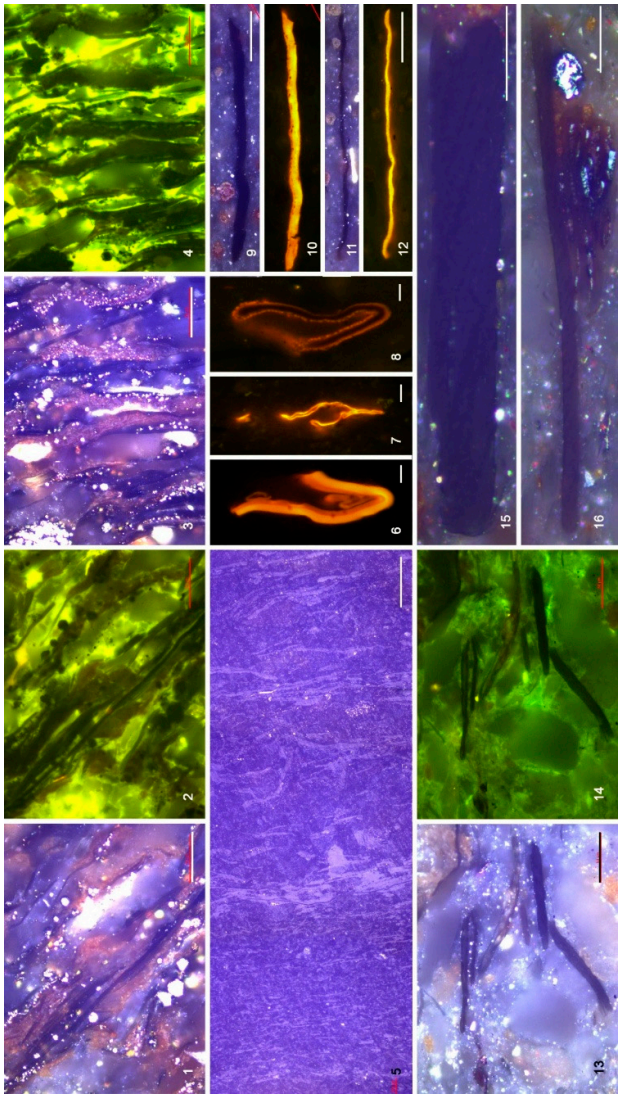

Figure 12. 1-5 are from organic microfacies (B) 20 –A/B. 6-16 are from organic microfacies (B) 20 –C. 1-4, 13, 14 scale bar 50μm, 6-8 scale bar 10 μm, 5 scale bar 200μm. 1-4 Plant remains organic articles, they are laminated with the rock matrix and aligned with pyrite, 1, 2 same field, 3, 4 same field, 1, 3 incident white light, 2, 4 incident blue light. 5 large field of thinly laminated organic particles in photomicrographs of 1-4. 6-8 spores with orange color in incident blue light. 9-12 cutinite, 9, 10 same fields, 11, 12 same fields, 9, 11 incident white light, 10, 12 incident blue light. 13 -16 Structured plant remains with braided like texture, thinly laminated with rock matrix, the particles have n-o fluorescence color, 13, 15, 16 in incident white light, 14 in incident blue light.

Sample 20-C was collected from a depth of 9371 ft (Figure 2). The organic particles in this sample were markedly different from those found three feet lower despite they also had a faint grayish brown color in white incident light (Figure 12 (13-16)). Notably, some of these particles are plant remains with a distinct lath-like shape (5.6%) (Figure 12 (13-16)). They were still parallel to the lamination of the rock matrix but had a distinctive thickness, definitive boundaries, and cell structure (Figure 12 (13-16)). These organic particles had a braided structure that extended along the entire length of the particle (Figure 12 (15-16)). These particles had no fluorescence in blue light (Figure 12 (13-16)) and were classified as vitrinite. Similar dark brown lath shaped particles that showed strong orange fluorescence were identified as cutinite (Figure 12 (9-12)). These particles were less abundant (3.4%) and well recognized with their dark brown color in white light (Figure 12 (9-12)). Sporinite was also well recognized as having orange fluorescence color (Figure 12 (6-8)). Different types of spores (1%) were observed and the most abundant are the thick forms (Figure 12 (6)). A similar

 doi:10.20944/preprints202603.1900.v1

distribution was found in the palynofacies analysis where the spores (54.7%), the translucent phytoclasts (28.7%), and non-translucent ones (3.7%) were the dominant palynofacies classes (Figures 3 and 6) from the total counts. Marine palynomorphs including acritarchs (0.35%), chitinozoans (0.53%), prasinophytes (0.35%), and scolecodonts (0.17%) occurred in minor abundances (Figures 3 and 6). The organic matter density was 9.0%. The rock matrix was characterized by occurrence of carbonate microfossils that had a well-developed ornamentation consisting of radial spikes and segments with internal concentric core cavity (Figure 11 (2-10)). These particles did not include any organic substances and ranged in size between 10 to 25 μm (Figure 11 (2-10)). They were abundant in the rock matrix and did not show orientation with respect to the mineral grains. These particles are like the tunicate spicules recorded previously since Cambrian and up to Recent [36,37]. The tunicates are like sea squirts belonging to the Ascidiaceae Class (primitive vertebrates). The tunicates have soft bodies that don't promptly fossilize and this is reason why they are rare in the fossil record [36]. Only small spicules that stiffen in the soft tissues are usually found in the sediments as sporadic grains of microfossils and are known as Ascidian spicules [37]. This is the first record of these spicules in Egypt and Africa in this age. The lath-shaped plant remains particles were found to be parallel to the bedding plan; however, there was no lamination in this organic microfacies, and the rock matrix was massive (Figure 11 (2)). The rock grains in these samples were coarser than the previous samples.

Sample 14-A was collected from 7707 ft (Figure 2). These organic microfacies are like the 20-A/B organic microfacies and were enriched in terrigenous organic matter like vitrinite (3%) and liptinite (6.0%) (cutinite and sporinite) (Table 2, Figure 13). The plant remains in this organic microfacies was represented by vitrinite that had gray color in incident white light (Figure 13 (7-11)). Cutinite was common in these organic microfacies (Figure 13 (4)). Sporinite was present in low concentrations (Figure 13 (9)). Palynofacies analysis revealed similar distribution of the organic matter classes whereby spores (43.7%) and translucent phytoclasts (36.4%) were the most abundant (Figure 3). Marine organic matter was scarce in these organic microfacies. The organic matter density reached 10.0%. There were no mineralic microfossils in the organic microfacies. There was a prominent alignment of organic particles including the vitrinite and cutinite with the rock matrix lamination (Figure 13 (1 and 2)). These sheets were present as thin layers of high organic density reflecting periodical (seasonal) changes in their input (Figure 13 (1-2)).

Low organic density organic microfacies C: These organic microfacies include four samples (18-A, 16-A, 15-B and 15-A) (Figure 6). Sample 18-A was collected at a depth of 8968 ft from the siltstone bed (Figure 2). This organic microfacies is like the organic content of the organic microfacies 19-A where the major component is the chitinous organic sheets (7.9%) (Table 2; Figure 14 (1-11)). However, the sheets that were detected in these organic microfacies occurred in thinner and successive layer groups (Figure 14 (1-4, 7, 9)). The sheets were straight (length about 1 mm) and exhibited less bending and wrinkling compared to those observed in 19-A (Figure 7). Despite exhibiting identical optical characteristics (Figure 14 (5-13)) that suggest an identical chemical composition, some sheets in 18-A demonstrate a homogeneous composition throughout their thickness, lacking any layering (Figure 14 (8)). However, some pores (Figure 14 (11) were noticed in the sheet section that are like these notices in the chitinous sheets observed by Goodarzi [38; Figure 3 (A)]. Some sheets exhibited splitting along weak surfaces, which can lead to the complete separation of a thick sheet into two thinner sheets (Figure 14 (1-4)). This was particularly evident where the thin sheets remain connected at both ends and display morphological symmetry (Figure 14 (1-3)). Some sheets that were leveled parallel to sheet surface are particularly important because they displayed morphological features that could point to their origin (Figure 14 (5 and 6)). One sheet had circular holes that were like those in eurypterids recorded in Devonian strata throughout the Gondwana in general and Egypt in particular [4,10,39–43]. Typical sheets were also recorded in the Sifa-1X well in Givetian age in the polished rocks of the palynofacies type B that indicate deltaic settings [10]. The presence of eurypterids in these organic microfacies confirms their occurrences in microfacies of 19-A based on similarity of their optical characteristics. The other macerals are represented by acritarchs and prasinophytes that were detected in minor quantities The organic matter density was 7.9%.

 doi:10.20944/preprints202603.1900.v1

Calcareous tunicate spicules became prominent in these organic microfacies with clear concentric lines and radial spikes that are typical of the general morphology of this group of microfossils, like those recorded in the Pliocene by Bankole et al. [37] (Figure 14 (12-20)). A direct comparison with a similar Devonian record is not possible because of the absence of literature at this age. Thus, it is likely the first record of Ascidian spicules in the Devonian. The grains of the tunicae spicules showed the typical mace-like shape and concentric lines of growth that are found in Ascidian spicules in other ages such as Pliocene and Quaternary [44] (Figure 14 (12-20)). Some grains overlapped and this is also typical of the Ascidian spicules [44]. The spicules showed yellow fluorescence, which possibly reflects their calcareous nature. Based on the morphological variations, these grains can be classified into different taxa. The rock matrix was massive; however, the chitinous sheets were parallel to each other and to the bedding plane (Figure 14 (10)). The distribution of the tunicate spicules was sporadic.

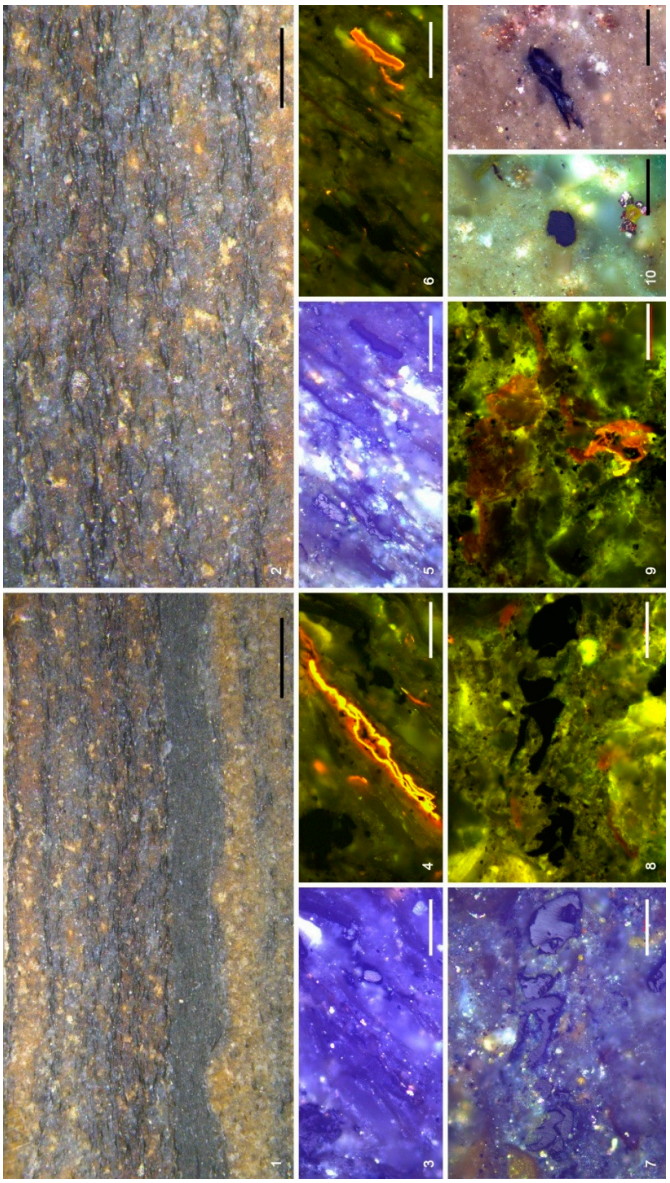

Figure 13. Organic microfacies (B) 14-A. 1, 2 scale bar 500µm. 3 -9 scale bar 50µm. 10, 11 scale bar 30 µm. 1, 2 Large field of the rock surface showing the thin lamination of the organic matter and rock matrix. 3-6 Thin lamination of cutinite, vitrinite and sporinite with rock matrix. 17, 10, 11 Rounded vitrinite grains. 9 Cutinite. 4, 6, 8, 9 are in blue incident light and 1, 2, 3, 5, 7, 10, 11 are in white incident light.

 doi:10.20944/preprints202603.1900.v1

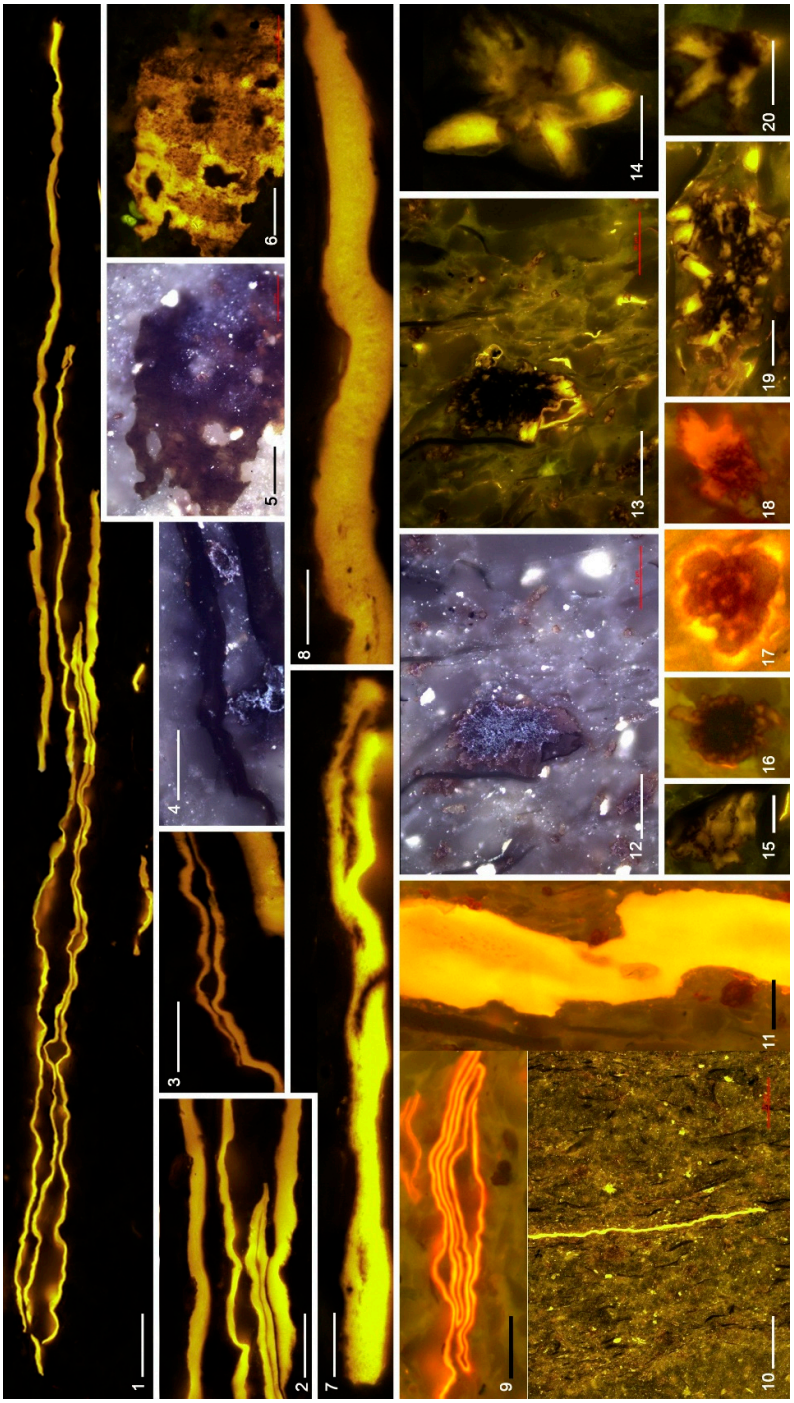

Figure 14. Organic microfacies (C) 18-A. 1, 12, 13 scale bar 50µm, 2-6 scale bar 30µm, 7, 8, 11, 14, 20 scale bar 10µm, 9 scale bar 50µm, 10 scale bar 200µm. 1-11 chitinous sheets showing different layering and lamination with rock matrix. 5, 6 chitinous sheets with pores. 12-20 Tunicate spicules with different forms. All in incident blue light except 4, 5, 12 are in white incident light.

Sample 16-A was collected at a depth of 8203 ft from Ironstone bed (Figure 2). No organic matter was detected in this core sample. The microscopic examination revealed the presence of iron-rich coated grains (Figure 15). These coated grains exhibited a range of sizes and types (Figure 15). Size analysis of 139 coated grains identified three distinct size groups (Figure 16a). The first group ranges in size between 50 and 318 µm (mean=183; count=120) and it is the most abundant group. This group comprises all the finely laminated concentric tangential coated grains representing the type 4 of ooid

 doi:10.20944/preprints202603.1900.v1

bar (Figure 15) according to the classification of Flügel [45, p. 121]. The second group ranged in size from 318 to 583 µm (mean=420; count=16) (Figure 16a). This group of grains was also classified as finely laminated concentric tangential ooids (Figure 15). The last group is the largest in size (1060-1484 µm, mean=1336, count=3) (Figure 16a). In addition to the finely laminated concentric tangential coated grains (ooids type 4), this group also included aggregate coated grains (aggregated grains type 4) that contained several smaller ooids and skeletal grains inside the single coated grains (Figure 15). The grains were mostly rounded in the section, but the larger aggregate grains were elliptical in shape (Figure 15). The thickness of the coat in the first group is like the thickness of the last coat of the third group (Figure 15). Some of the aggregate grains were eroded showing broken peripheries (Figure 15). The rock was composed of homogenous coated grains of different compositions and textures.

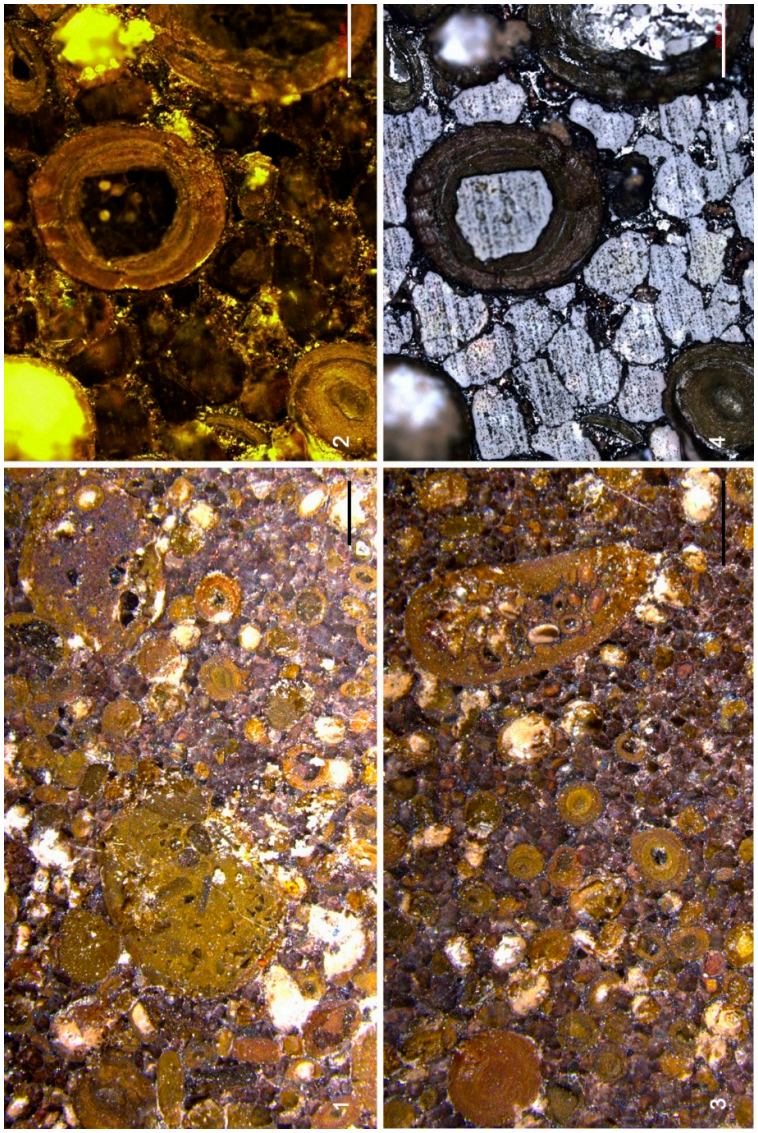

Figure 15. Organic microfacies (C) 16-A. 1, 3 scale bar 500µm. 1, 2 scale bar 50µm. 1,3 Large fields of rock section photomicrographs showing the iron oxide coated grains. 2, 3 same microscopic field showing the thin lamination of the coated grains, 2 is in blue incident light and 4 is in white incident light.

 doi:10.20944/preprints202603.1900.v1

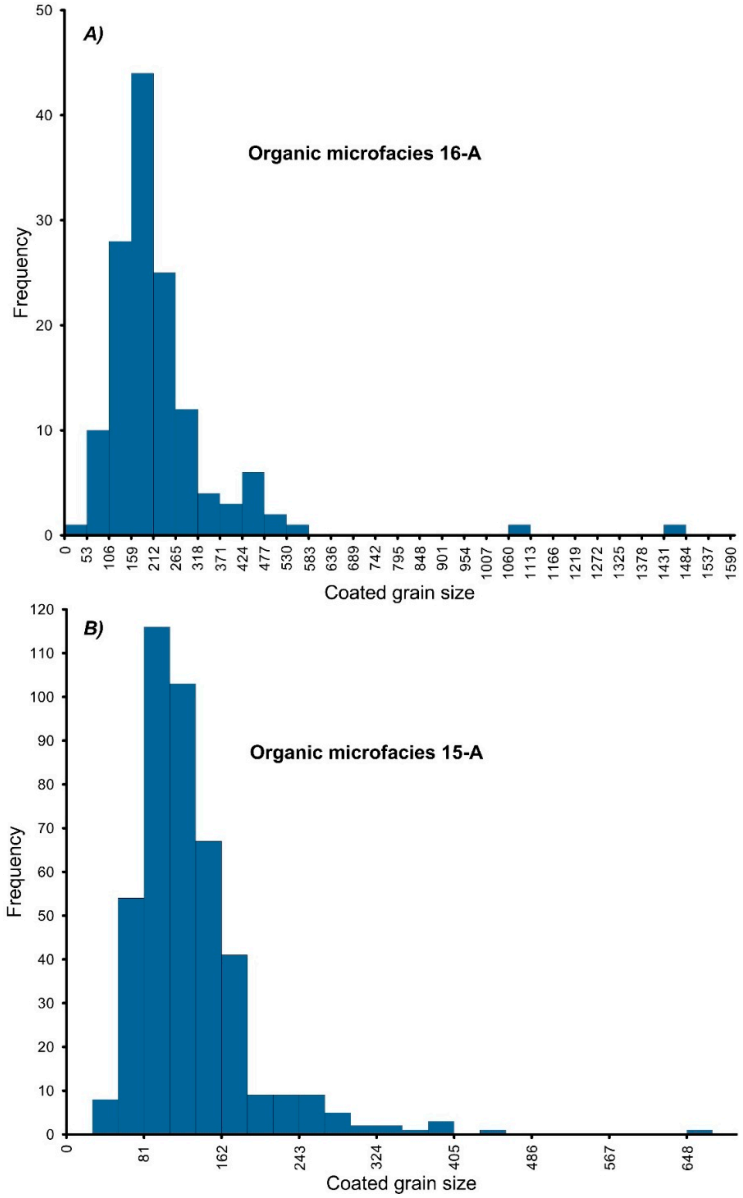

Figure 16. Size variations of the coated grains from organic microfacies C, a) 16-A b) 15-A.

Sample 15-B was collected at a depth of 7942 ft from the dark shale bed (Figure 2). The organic matter was enriched in alginite (Table 2). The alginite included acritarchs and prasinophytes (Figure 17 (9-12)). Three new components were recorded in 15-B organic microfacies of liptinitic nature (0.07%) (Figure 17 (1-3, 4-8, 15-22)). The first component comprised structured particles of unidentified origin. The particles had strong orange and yellow fluorescence color and brown color in white incident light (Figure 17 (2-8)). These particles were covered with a thin film of pyrite. The second component consisted of massive resinous particles that had yellow fluorescence (Figure 17 (15, 16)). The third component encompassed alginite-like particles that were colorless in incident white light and showed orange color in blue light (Figure 17 (17-22)). These alginite-like particles were circular to cylinder shaped and had cotton candy texture. The organic matter presented 0.1% (Table 2, Figure 6). This organic microfacies facies is distinguished by the occurrences of the foraminiferal test (Figure 17 (13-14)). The foraminifera were likely of calcareous origin, the original test was dissolved, and the internal chambers were filled with calcareous matter (Figure 17 (13-14)). The foraminiferal tests had a biserial arrangement in the earlier stages that converted to uniserial in the last two stages. The rock matrix was massive.

 doi:10.20944/preprints202603.1900.v1

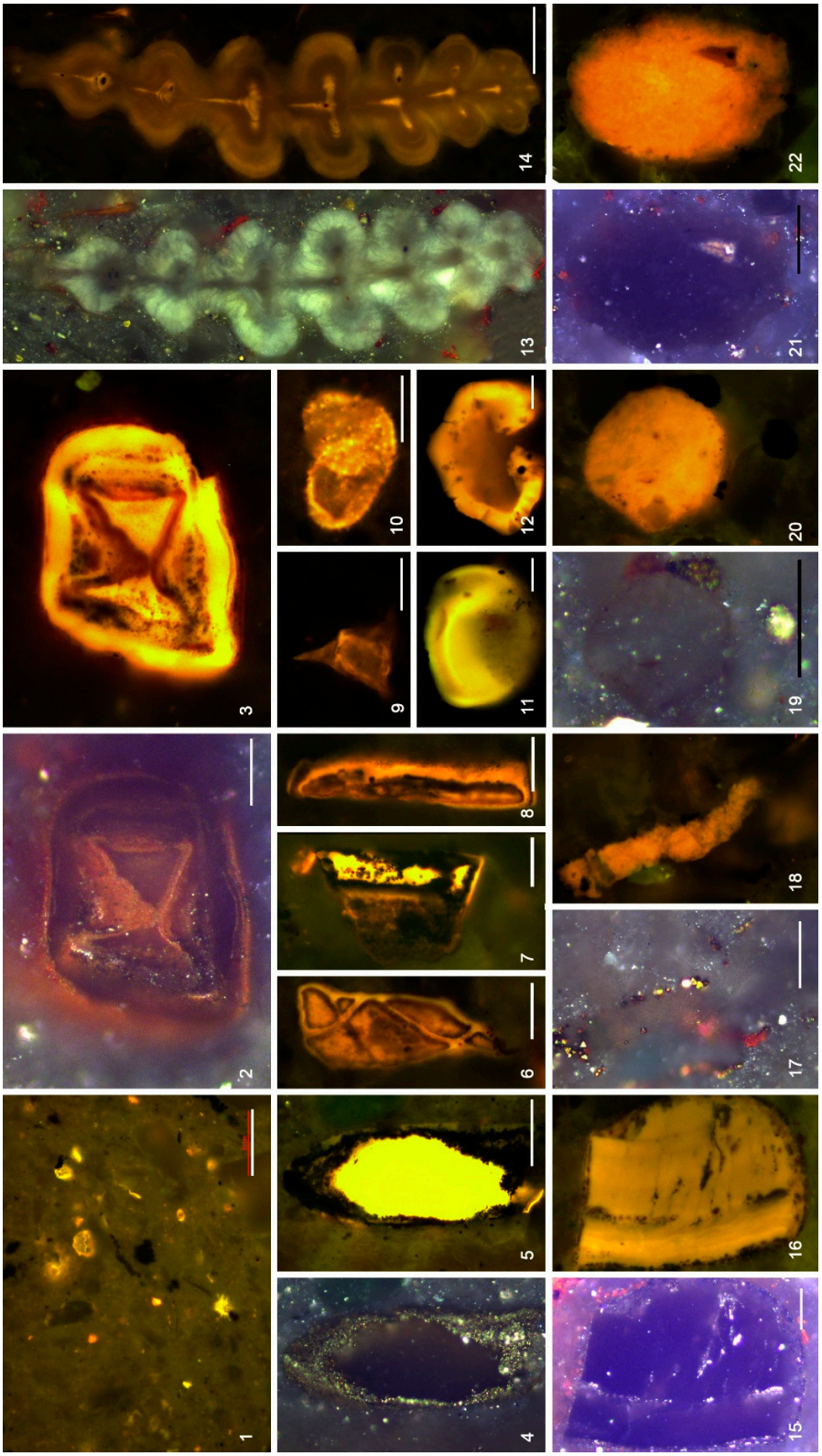

Figure 17. Organic microfacies (C) 15-B. 1, 2, 3, 13, 14 scale bar 50µm. 4-8, 15-22 scale bar 25µm. 9-12 scale bar 10µm. 9-12 scale bar 10µm. 1 Large field showing the nature of organic matter distribution in the organic facies. 2-8 Organic matter of un-identified origin. 9, 10 Acritarchs. 11, 12 Prasinophytes. 13, 14 Foraminifera., 15, 16 resinous organic particle. 1-22 Bituminite. All photomicrographs are in blue incident light except 2, 4, 13, 15, 17, 19, 21 are in white incident light.

 doi:10.20944/preprints202603.1900.v1

Sample 15-A was collected at a depth of 7948 ft from the ironstone bed (Figure 2). The observed organic matter was mostly alginite (4.4%) with minor occurrences of sporinite and inertinite (0.6%) (Table 2; Figure 3). The organic matter content was 6.0% (Table 2). The composition of the ironstone in this part of the core 15 witnessed significant changes in the texture of the coated grains that were in general finer than this in the lower part of the ironstone bed in core 16-A (Figures 18 and 19, Figure 16b). The significant changes include the presence of oncoids and occurrence of thin layering (Figure 18). The oncoids were distinguished with thick cortex formed by irregular and non-concentric partially overlapping micritic lamina (Flügel [45, p. 100]). The oncoids ranged in size between 100 to 300 μm (Figures 18 and 19, Figure 16b). The oncoids had ellipsoid to circular shape and occasionally diffused with each other forming one larger grain (Figures 18 and 19). The ellipsoidal cross section reflects the discoid shape of the oncoid whole grain. The oncoids were arranged with their long axis parallel to a general bedding plane (Figure 18). Analysis of the oncoid sizes indicated three distinctive groups (Figure 16b). The first group included oncoids that ranged in size between 32 μm and 189 μm (count=391; mean =115 μm) (Figure 16b). The second group ranged in size from 189 μm to 297 μm (count=30; mean =237 μm) (Figure 16b). The third group comprised the size range of 297-675 (count=10; mean =395 μm) (Figure 16b). However, the size variations are related to the layers of oncoids whereby each layer contained relatively sorted sizes (Figures 18 and 19). The sorting of the oncoids sizes can be measured by the standard deviation. The lower layer is 1034 μm and has relatively larger oncoids and higher standard deviation (count=151; mean =141 μm, standard deviation=74) (Figure 18). The middle layer is thick (1568 μm) and has the finest oncoids (count=170; mean =119 μm, standard deviation=39). The oncoids in the upper layer (597 μm) became larger again with higher standard deviation (count=110; mean =131 μm, standard deviation=72) (Figure 18). The aggregate grains still exist but were not common (Figure 18). The lamination was noticed in the rock matrix between the oncoids lamina and rock matrix (Figures 18 (1) and 19). The lamination was also observed between the rock matrix and the organic particles including sporinite and alginite (Figure 18 (3-11)).

 doi:10.20944/preprints202603.1900.v1

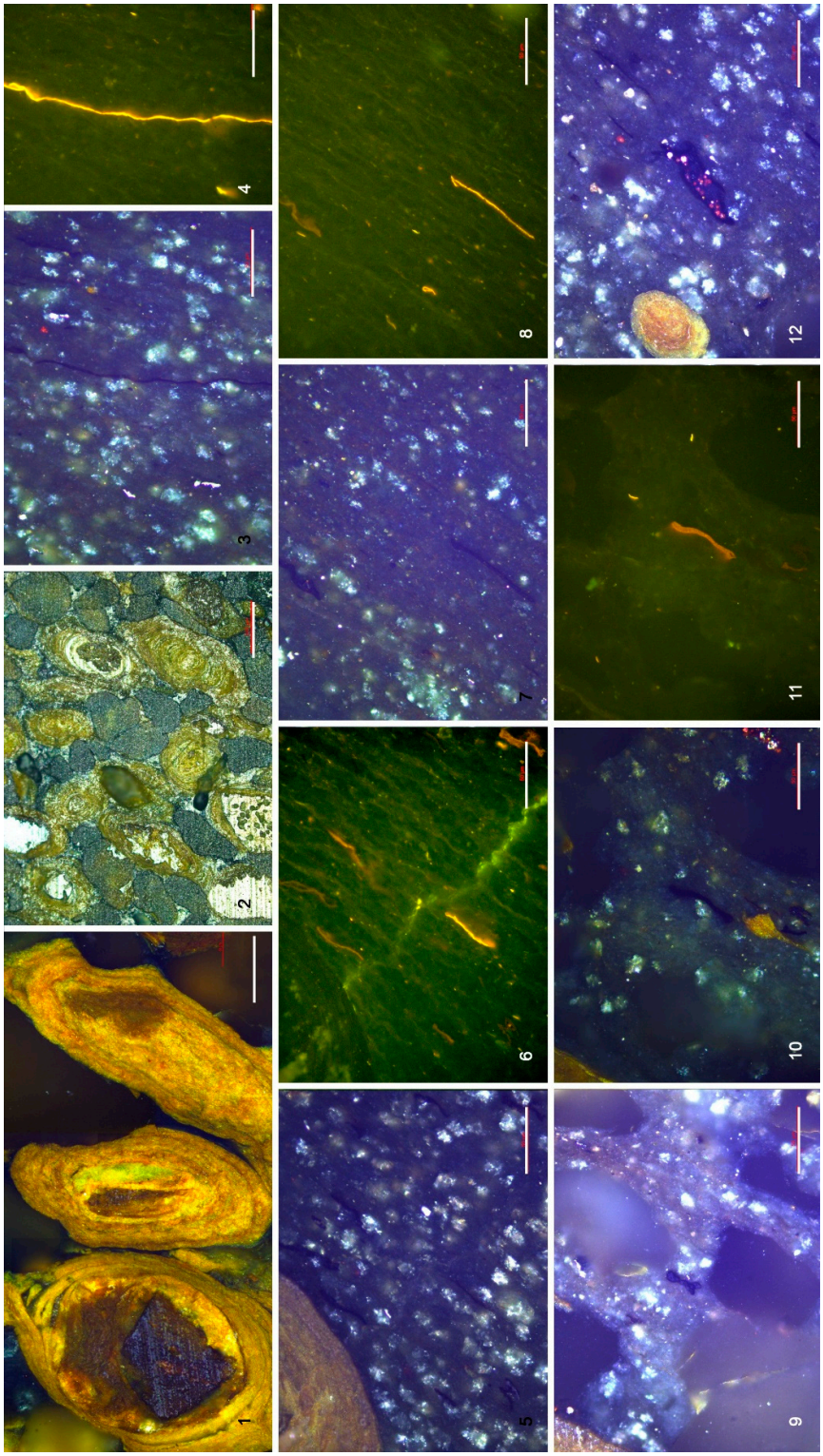

Figure 18. Organic microfacies (C) 15-A. 1-3 scale bar 500μm. 1-3 Large fields of rock section photomicrographs showing the layers of iron oxide coated grains.

 doi:10.20944/preprints202603.1900.v1

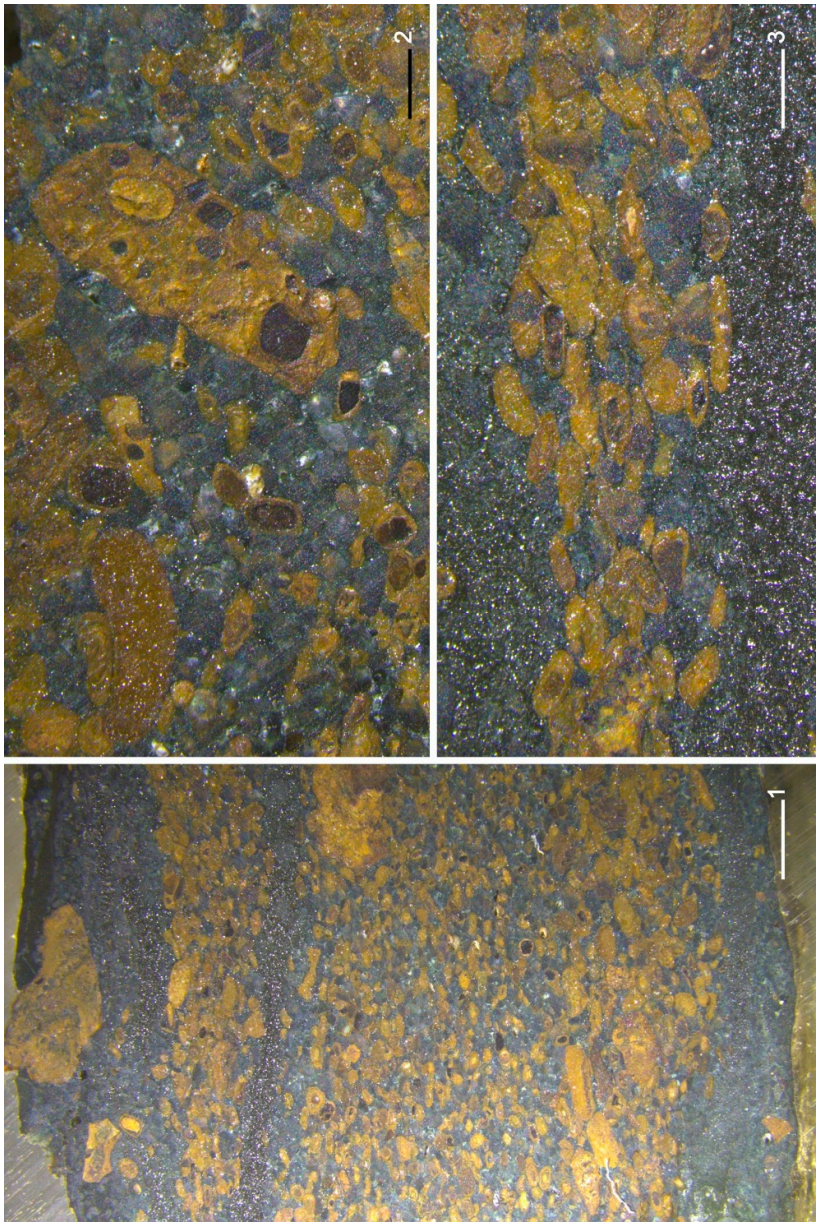

Figure 19. Organic microfacies (C) 15-A. 1, 3-12 scale bar 50µm. 2 scale bar 200µm. 1 The lamination of the oncoid grains. 2 overview of the oncoid and rock matrix grains. 3-12 lamination of the rock matrix with organic matter. 3, 4 Cutinite. 5-8 Alginite. 9 Vitrinite. 10, 11, 12 Sporinite. 1, 2, 3, 5, 7, 9, 10, 12 in white incident light. 4, 6, 8, 11 in blue incident light.

5. Discussion

5.1. Paleoenvironmental Analysis of Organic Microfacies

5.1.1. Organic Microfacies A

The chitinous arthropod sheets and other remains are found in a variety of environments including aquatic terrestrial and marine habitats [41]. The mixture of cutinite and sporinite that are usually found abundant in moderate proximity of fluvio-deltaic sources with large arthropod sheets indicate a proximal environment. The excellent preservation of the abundant sheets is usually linked to low oxygen conditions [30] during the deposition of the 19-A sample. The remarkable characteristics of this organic microfacies are the occurrence of wrinkled chitinous sheets of the arthropods with strong fluorescence that produce a wafer-like structure with rock matrix. These

 doi:10.20944/preprints202603.1900.v1

sheets are like the chitinous zooepidermis fragments recorded by Goodarzi [38] from the Anxiety Butte coal zone, Ravenscragg Formation, exposed at Ravenscragg Butte, Saskatchewan, Canada. Although both types of sheets have two layers, the sheets recorded in the present study are homogenous and do not include fibers or difference in fluorescence between both layers as these recorded by Goodarzi [38]. Fluorescent arthropod remains were also detected previously in the palynofacies analysis of the Devonian rocks in the Western Desert of Egypt but the presence of layers within each sheet was not recorded before [3,10].

Sample 18-B represents an acute shift of environmental settings. The density, diversity, and abundance of organic matter is like the samples recorded in the Sifa-1X well in Faghur Basin in the Western Desert. These similar polished rock samples belong to palynofacies type A that represents shelf to distal prodelta slope [10]. This environmental setting is characterized by high productivity, low oxygen, and low sedimentation rates [30,46,5,47,10,48). The main characteristic of the condensed section, deposition in distal part of the basin and relatively high sea level is the low sedimentation rate that resulted from an increase in the basin accommodation [30,49]. These microfacies are also the nearest to the maximum flooding surface of the sequence DevSeq2 [3] (Figure 1B). This organic microfacies is highly distinguished from the influx of marine palynomorphs and spores. Sample 18-B is highly correlative to the samples of the condensed section recorded in sequence 2 (Seq2) in the Middle Devonian [10]. Moreover, the samples belong to the distal oxic shelf palynofacies type as recorded by Makled et al., [3].

In sample 17-A, the lamination and influx of the marine palynomorphs are like organic microfacies 18-B. The condensation and relative low sea level continued from the 18-B organic microfacies to this part of the Givetian. However, the tunicate spicules are not documented in the 17-A organic microfacies and this is an essential difference that indicates significant change in sea water characteristics that can be linked to nutrition availability [50]. The tunicates are filter feeders that pass water through pharynx and collect the phytoplankton including algae and acritarchs [51]. Accordingly, the decreasing size and abundance of algal grains like prasinophyte and acritarchs that indicate significant decline in productivity can affect the abundance of tunicates [30]. These organic microfacies are positioned at the maximum flooding surface of the DevSeq3 (Figure 1B) [3].

5.1.2. Organic Microfacies B

The high relative abundance of the terrigenous organic matter detected in polished rock fragments and palynofacies indicate highly proximal environmental settings, especially when absence of marine organic matter and other marine microfossils is considered [30]. However, other environmental conditions can be outlined from the rock fabric. Within the scale of 1 mm, the thinly laminated rock fabric reflects low energy deposition. If accompanied by parallel organic flakes (sheet-like particles), it indicates the deposition from suspension [47,52]. The degree of lamination is a good indicator for oxygen in the environment because it reflects the low or absent bioturbation [30,47]. The faint lamination in the present samples is similar to oxygen level 4 facies on the scale of Röhl and Schmidt-Röhl [47]. These environmental settings are often available in the distal side of the basin, however, with the mineral grain size resembling the thick lamination in near shore recorded by O'Brian [52] that is characterized with low velocity bottom-flowing currents. In conclusion, these organic microfacies are deposited in a deltaic environment that received a major supply of terrigenous plant remains [30]. The distal side of the delta platform to delta front with low oxygen conditions and below wave base is probably the specific environment setting. The marine influx is also represented with the tunicate spicules that are usually found in shallow water to deep marine environments [53].

5.1.3. Organic Microfacies C

These organic microfacies indicate open marine or distal environment. In 18-A sample, the open marine settings are favored because of lacking the terrigenous organic matter [30] and because of the presence of tunicate spicules and eurypterids that thrive in shallow marine waters [41,53].

 doi:10.20944/preprints202603.1900.v1

In sample 16-A, the different size and erosion of the coated grains indicate several stages formation through formation- shallow burial – reworking and reformation [54,55]. This is confirmed by the absences of thin laminations in this sample, which indicate continue active agitation during the formation of the coated grains. Moreover, continuous agitation is evident by the absence of organic matter in this sample (Table 2). The formation of rich iron coated grains was the subject of several studies that dealt with ironstones from different ages [54–59]. These studies suggested different mechanisms for ironstone deposition, especially these that include coated grains based on the source of the iron. The sediments of Pragian - Emasian to Givetian ironstones from the Parnaíba Basin (Brazil) are represented by authigenic coated phosphatic iron silicates that are related to normal regression under lowstand and highstand system tracts. The Fe is mostly contributed to the basin through river discharge and maintained high through cyclic upwelling [56]. The Fe source of other hematite rich stratiform ironstones from South China that include coated grains is from continental metals but with variable involvement of hydrothermal flows in venting sea floor in fault bounded basins within shallow marine environments [59]. The last mechanism is the formation of ironstone in the non-depositional/low sedimentation rate period (condensation) in the transgression of high sea level on the scoured surface of siderite hard ground (Ordovician, Western Europe, 60). The source of the Fe is also from input that resulted by terrestrial weathering, and the concentration begins to increase during the non-deposition of the other detrital sediments. In this case, the degradation of organic matter becomes widespread because of deposition in oxic and suboxic conditions [60]. The 16-A organic microfacies are deposited under similar scenario to the condensation model of Young [60]. This indicates that the condensation detected in the previous organic microfacies 18-B and 17-A reached its maximum leading to sedimentation of ironstone recorded in the 16-A organic microfacies. The absence of organic matter is because deposition in oxic conditions and degradation are intensified by the occurrences of several events of reworking and deposition.

Sample 15-B shows completely different environmental settings that witness the return of terrigenous sediments and termination of condensation (Figure 3). The presence of foraminifera, along with the dominance of marine organic matter such as alginite and acritarchs signifies deposition in an open marine environment under suboxic conditions [30]. The bituminite is well preserved demonstrating low oxygen conditions [30]. Sample 15-A witnessed the extension of condensed section paleoenvironmental settings. The lamination of the oncoid, lamination of the rock matrix, and fewer occurrences of aggregate grains indicate limited reworking of the oncoids after their formation [61–64]. This is also additional evidence that these oncoids are microbialites that are formed by in-situ microbial growth in low energy settings [61–68]. This enhances the preservation of organic particles that were observed frequently in the rock matrix around the oncoid. The organic particles also arranged parallel to the lamination direction of the rock matrix, which should happen in occasional calm deposition of the rock matrix after formation of the oncoid. Some sporinite particles have pyrite fillings that indicate low oxygen conditions. The deposition generally occurs in shallow open water conditions.

5.2. Evolution of Organic Facies Through the Devonian and Their Significance

The integrated analysis of the Devonian organic microfacies provides a high-resolution framework for understanding basinal evolution and cyclic sedimentary changes. By utilizing organic petrography to define these microfacies, this study demonstrates that each organic microfacies serves as a biological and textural fingerprint. Unlike traditional bulk geochemical and palynofacies methods, organic microfacies analysis captures the interaction between organic macerals, mineral microfossils, and rock textures [69]. This approach allows for a compehensive interpretation of paleoenvironments than Rock-Eval pyrolysis and palynofacies alone provide. It directly observes the preservation state and spatial arrangement of kerogen within the rock matrix [70].

This study shows how the Devonian organic microfacies changed during the time span of 21 myr in total thickness of 1673 ft (Figures 2 and 3). The earlier organic microfacies in the Emsian started with plant remains that were characterized by sheet-like particles that were stratified with the

 doi:10.20944/preprints202603.1900.v1

lamination of the rock matrix in organic microfacies 20-A/B. These particles were associated with sulfide minerals and were rapidly replaced with lath-shaped particles. The lath-shaped particles showed more complicated structure but kept their stratification with the rock matrix and were accompanied by more diverse organic assemblage in organic microfacies 20-C. The change included the appearance of calcareous microfossils of tunicate spicules. These changes reflect variations of the marine and terrestrial populations without significant modifications of depositional environment that allowed for the formation of thin laminations in proximity to the terrigenous organic matter sources.

The similarity of the organic particles can be noticed through the organic microfacies of 19-A, 18-A, 18-B and 17-A, however with different density, abundance, and diversity indicating constant shift to more distal environmental settings. These microfacies represent different degrees of low sedimentation rates reaching condensation in organic microfacies 18-B. The sediment starved sections are used frequently for stratigraphic correlation, especially in the routine sequence stratigraphic classification of the rocks section [71,72]. The organic microfacies are also noticed in the Givetian rocks from the Faghur Basin in the Western Desert of Egypt [10]. The increasing of the marine organic matter is noticed also in Eifelian, Givetian, and Frasnian from other locations in the Gondwana, such as in the Pimenteira Formation in Brazil, which represents high sea level (Abram and Holz, 2020). The rocks of Pimenteira Formation contain many ironstone beds that comprise coated grains like these recorded in organic microfacies 16-A and 15-A. The evidence of sediment condensation in the present study in the time of the Givetian is supported by the presence of the ironstone beds that represent the peak of sediment starvation. Although the formation of the coated ironstone involves many mechanisms, sediment condensation remains the basic process that led to the production of the iron oxide coated grains [72]. The sediments that belong to marine high sea levels in the middle Devonian that are topped with ironstones are also found in many areas in Libya. They could form the basis of accurate intra-basinal stratigraphic correlation in the Faghur Basin in Egypt and the Cyrenaica and Murzuq basins in Libya. Coeval sediments are found in the sandstone of the Awaynat Wanin Formation in Wadi Shatti in the Murzuq Basin with large deposits of low-grade oolitic ironstone [73]. They are also found in the transgressive system tract of the Frasnian depositional sequence 6 in Wadi Dabdab in the uppermost part of the Quttah Formation [74], which indicates the reoccurrence of condensations in North Africa. The same occurs in the Famennian sediments from Mecheri Abdelaziz in Algeria [75]. The equivalent sediments can be tracked to south China where oolitic ironstones are found in the Middle Devonian sediments of Ningxiang type deposits [59]. The stratification of alginite and sporinite with the oncoid in thin lamination of the rock matrix in organic facies 15-A shed light on the mechanism involved in the formation of these oncoids and their microbial origin.

After the widespread high sea level prevailed from Eifelian to Givetian, the organic microfacies recorded in the Frasnian organic microfacies 14-A indicated proximal environmental settings that carried similar characteristics to those of organic microfacies 20-A/B. The same distribution pattern appeared 21 myr later in the Frasnian. Similar plant particles stratified with rock lamination, but with additional vitrinite, sporinite, and cutinite in organic microfacies 14-A, are indicative of another evolutionary stage at that period. This represents a major cycle of sedimentation that repeated the depositional environment conditions and pattern of sedimentation even with different organic components. These changes represent the interaction between the organic matter evolution in terrestrial and marine areas, their rate of delivery to the basin, and the ability of the sediment to bury and preserve the organic matter [5,30,46]. The evolution of organic matter determines the new compounds that will be transferred to the basin, their productivity, and their sensitivity to destruction in the journey to burial location and its fate after burial. The ability of the sediment to bury and preserve the organic matter depends on the rate and type of sedimentation and oxygen content, both of which are controlled by the sea level and proximity to the source of the organic matter.

The organic microfacies discussed are the net result of the complicated interaction between these factors and processes. This interaction produces the characteristics of each organic microfacies. Each

 doi:10.20944/preprints202603.1900.v1

organic microfacies has its own identity that makes their repetition indicative of the cyclical pattern. This will increase their value in stratigraphic correlation between wells. Furthermore, the analysis of the cyclical patterns of sequence stratigraphy that is based on organic microfacies will be of greater accuracy because it depends on the repetition of the conditions that could lead to certain distribution patterns of organic matter and interaction with the rock matrix.

6. Conclusions

This study examined and documented organic microfacies from the Devonian Zeitoun Formation in the Faghur-1 well. These microfacies, sampled from cores spanning a 21-million-year interval from the Emsian to the Frasnian, provided significant insights into the Faghur basin's geological history, including organic matter evolution and its interaction with the rock matrix. Ten distinct organic microfacies were identified within twelve parasequences, delineated through lithological variations observed in the cores and microscopic examination. The microfacies indicate proximal Emsian environments, transitioning to distal, high sea level conditions throughout the Eifelian and Givetian, marked by abundant marine organic matter. Sediment condensation culminated in the formation of ironstone enriched in coated grains by the late Givetian. The Frasnian marks the onset of a new major cycle characterized by return to proximal environmental settings, similar to those observed in the Emsian. These organic microfacies provide a precise fingerprint, representing a unique assemblage of organic matter and specific rock matrix interaction patterns, enabling intra-basinal stratigraphic correlation. Several microfacies identified in this study correlate with contemporaneous stratigraphic events documented in Gondwanan regions, including Libya and Brazil. These characteristic organic microfacies offer a powerful tool for resolving stratigraphic challenges within the complex subsurface geology of the Faghur Basin, thereby aiding petroleum exploration efforts.

Author Contributions: Conceptualization, W.A.M.; Methodology, W.A.M.; Software, W.A.M.; Validation, A.I.A.-J., F.A.; Formal analysis, W.A.M., A.K., A.I.E., M.M.E.G.; Investigation, W.A.M., A.K.; Data curation, W.A.M., A.I.E., M.M.E.G.; Writing-Original draft, W.A.M., A.K., A.I.E., M.M.E.G.; Supervision, N.A.; Writing-review and editing, A.I.A.-J., N.O., T.G., F.A..

Funding: The authors extend their appreciation to the King Saud University for funding through Ongoing Research Funding program (ORF-2026-1120), King Saud University, Riyadh, Saudi Arabia.

Acknowledgments: The Egyptian Petroleum Research Institute provided the organic petrography studies.

References

1. IHS Markit. Petroleum exploration and production database. Houston, Texas, IRS Energy, Inc. **2018** (database available from IHS Energy).
2. EGPC (EGYPTIAN GENERAL PETROLEUM CORPORATION), **1992**. *Western Desert, oil and gas fields*. EGPC, Cairo, Egypt, 431 pp.
3. Makled, W.A.; Mostafa, T.F.; Mousa, D.A.; Abdou, A.A. Source rock evaluation and sequence stratigraphic model based on the palynofacies and geochemical analysis of the subsurface Devonian rocks in the Western Desert, Egypt. *Marine and Petroleum Geology* **2018**, *89*, 560-584.
4. Makled, W.A.; Hints, O.; Hosny, A.M.; Shahat, W.I., Gentzis, T. Exotic Devonian palynomorphs from the Sifa-1X well in the Western Desert, Egypt. *Palynology* **2021a,** *45*(2), 363-380.
5. Tyson, R.V. The "productivity versus preservation" controversy: Cause, flaws, and resolution. In: Harris, N. (Ed). Deposition of Organic-Carbon-Rich Sediments: Models, Mechanisms, and Consequences, SEPM Special Publication 82 **2005**, 17–33.
6. Stasiuk, L.D.; Osadetz, K.G.; Goodarzi, F.; Gentzis, T. Organic microfacies and basinal tectonic control on source rock accumulation; a microscopic approach with examples from an intracratonic and extensional basin. International Journal of Coal Geology, **1991**, *19*(1-4), 457–481.

 doi:10.20944/preprints202603.1900.v1

7. Al-Juboury, A.I.; Al-Auqadi, R.S.; Alarifi, N.; Shingaly, W.S.; Vincent, S.J.; Howard, J.P.; Vautravers, B.P.H. Petrography and geochemistry of the Late Devonian Pirispiki Formation in northern Iraq: Implications for Reservoir Characteristics and reconstruction of depositional environments. *Journal of African Earth Science* **2024**, *214*, 105240, https://doi.org/10.1016/j.jafrearsci.2024.105240
8. Al-Auqadi, R.S.; Al-Juboury, A.I.; Alkhafaji, M.W.; Alarifi, N.; Makled, W.A.; Rowe, H.; Zanoni, G.; Dettman, D.L. Depositional environments and thermal maturity of the hydrocarbon source rocks in the Devonian–Early carboniferous Ora Formation from palynological organic petrographic investigations in northern and western Iraq. *Journal of African Earth Science* **2024a**, *219*, 105400 https://doi.org/10.1016/j.jafrearsci.2024.105400
9. Al-Auqadi R.S.; Alkhafaji, M.W.; Al-Juboury, A.I.; Zumberge, A.; Alarifi, N.; Jarvie, D.; Zanoni, G.; Rowe, H. Organic geochemistry of the middle Paleozoic Ora Formation in Iraq: Implications for source rock assessment and hydrocarbon potentiality. Heliyon, **2024b**, *10*, e29782 https://doi.org/10.1016/j.heliyon.2024.e29782.
10. Makled, W.A.; Gentzis, T.; Hosny, A.M.; Mousa, D.A.; Lotfy, M.M.; Abd El Ghany, A.A., ... and Shahat, W.I. Depositional dynamics of the Devonian rocks and their influence on the distribution patterns of liptinite in the Sifa-1X well, Western Desert, Egypt: implications for hydrocarbon generation. *Marine and Petroleum Geology*, **2021b**, *126*, 104935.
11. Klitzsch, E. The Paleozoic. In: Said, R. (Ed.), The Geology of Egypt. **1990**, Balkema, Rotterdam, pp. 393–406.
12. Wanas, H.A. The Lower Paleozoic rock units in Egypt: an overview. Geoscience Frontiers, **2011**, 2(4), 491–507.
13. Keeley, M.L. Phanerozoic evolution of the basins of Northern Egypt and adjacent areas. Geol. Rundsch. **1994**, 83, 728–742.
14. Abd El Gawad, E.A.; Ghanem, M.F.; Makled, W.A.; Mousa, D.A.; Lotfy, M.M.; Temraz, M.G.; Shehata, A.M. Source rock evaluation of subsurface Devonian–Carboniferous succession based on palyno-organic facies analysis in Faghur Basin, north Western Desert of Egypt: a division of the north Africa Paleozoic basins. *Arabian Journal of Geosciences* **2019**, 12, 655. https://doi.org/10.1007/s12517-019-4802-5.
15. Ghori, K.A.R. Petroleum geochemical aspects of Cyrenaica, NE Libya. Third symposium on the geology of Libya. In: Salem, M.J., Busrewil, M.T., Ben Ashour, A.M. (Eds.), 7. Elsevier, Amsterdam, **1990**, pp. 2743–2756.
16. El-Arnauti, A.; Shelmani, M. Stratigraphic and structural setting. In: Thusu, B., Owens, B. (Eds.), The Palynostratigraphy of North-East Libya. *Journal of Micropalaeontology*, **1985**, *4*, 1–10.
17. ASTM (2015). D2797; Standard Practice for Preparing Coal Samples for Microscopical Analysis by Reflected Light. ASTM International: West Conshohocken, PA, USA.
18. Taylor, G.H., Teichmüller, Davis A., Diessel, C.F.K., Littke, R., Robert, P. (1998). Organic Petrology. Gerbrüder Borntraeger, Berlin, p. 704.
19. ASTM (2023 a). D2799-23; Standard Test Method for Microscopical Determination of the Maceral Composition of Coal. ASTM International: West Conshohocken, PA, USA.
20. ASTM (2023b). D7708-23a; Standard Test Method for Microscopical Determination of the Reflectance of Vitrinite Dispersed in Sedimentary Rocks. ASTM International: West Conshohocken, PA, USA.
21. International Committee for Coal and Organic Petrology (ICCP). (1998). The new vitrinite classification (ICCP System 1994). Fuel, 77(5), 349–358. https://doi.org/10.1016/S0016-2361(98)80001-6.
22. International Committee for Coal and Organic Petrology (ICCP). (2001). The new inertinite classification (ICCP System 1994). Fuel, 80(4), 459–471. https://doi.org/10.1016/S0016-2361(00)00102-2.
23. Pickel, W., Kus, J., Flores, D., Kalaitzidis, S., Christanis, K., Cardott, B. J., Misz-Kennan, M., Rodrigues, S., Hentschel, A., Hamor-Vido, M., and ICCP. (2017). Classification of liptinite—ICCP system 1994. International Journal of Coal Geology, 169, 40–61. https://doi.org/10.1016/j.coal.2016.11.004.
24. Ward, J. H., Jr. (1963). Hierarchical Grouping to Optimize an Objective Function. Journal of the American Statistical Association, 58(301), 236–244. https://doi.org/10.2307/2282960
25. Makled, W.A.; Baioumi, A.H.; Saleh, R.A. Palynostratigraphical studies on some subsurface middle Albian–early Cenomanian sediments from North Western Desert, Egypt. *Egyptian Journal of Petroleum*, **2013**, *22* (4), 501–515.

 doi:10.20944/preprints202603.1900.v1

26. Makled, W.A.; Mostafa, T.F.; Maky, A. Mechanism of Late Campanian–Early Maastrichtian oil shale deposition and its sequence stratigraphy implications inferred from the palynological and geochemical analysis. *Egyptian Journal of Petroleum*, **2014**, *23* (4).
27. Riding, J.B. A guide to preparation protocols in palynology. *Palynology*, **2021**, 45(sup1), 1–110. https://doi.org/10.1080/01916122.2021.1878305.
28. Mostafa, T.F. Palynostratigraphic Study of Devonian Rocks of the Western Desert, Egypt. Unpublished PhD thesis. Ain Shams University, Faculty of Science, Geology Department, **1997**.
29. El Shamma, A.A.; Mostafa, T.F.; Abdel Malik, W.M. Devonian spores from subsurface rocks in the Western Desert, Egypt. In: Proceedings of the 14th Petroleum Conference, EGPC, **1998**, pp. 1,451–1,465 Cairo.
30. Tyson, R.V. Sedimentary organic matter: organic facies and palynofacies. Springer Science and Business Media. **1995**.
31. Wang, H.; Lei, M.; Chen, Y.; Li, M.; Zou, L. Intelligent identification of maceral components of coal based on image segmentation and classification. *Applied Sciences*, **2019**, *9*(16), 3245.
32. Schindelin, J.; Arganda-Carreras, I.; Frise, E.; Kaynig, V.; Longair, M.; Pietzsch, T., ... and Cardona, A. Fiji: an open-source platform for biological-image analysis. *Nature methods*, **2012**, *9*(7), 676-682.
33. Skiba, M. The influence of the discrepancies in the observers' decisions on the process of identification of maceral groups using artificial neural networks. *Journal of Sustainable Mining*, **2016**, *15*(4), 151-155.
34. Rubo, R.A.; de Carvalho Carneiro, C.; Michelon, M.F.; dos Santos Gioria, R. Digital petrography: Mineralogy and porosity identification using machine learning algorithms in petrographic thin section images. *Journal of Petroleum Science and Engineering*, **2019**, *183*, 106382.
35. Witten, I.H.; Frank, E.; Hall, M.A.; Pal, C.J.; Data, M. Practical machine learning tools and techniques. In *Data mining*, **2005**, *2*(4), 403-413. Elsevier, Amsterdam, The Netherlands.
36. Wendt, J. The first tunicate with a calcareous exoskeleton (Upper Triassic, northern Italy). *Palaeontology*, **2018**, *61*(4), 575-595.
37. Bankole, S.; Buckman, J.; Stow, D. Unusual Components Within a Fine-Grained Contourite Deposit: Significance for Interpretation of Provenance and the Contourite Budget. Minerals, **2020**, *10*(6), 488. https://doi.org/10.3390/min10060488
38. Goodarzi, F. Chitinous fragments in coal. Fuel **1984**, *63*(11), 1504-1507.
39. Eisenack, A. Chitinozoen, Hystrichospharen und andere Mikrofossilien aus dem Beyrichia-Kalk; Senckenbergiana lethaea, 36, **1995**, 157- 188, pl. 1-5.
40. Taugourdeau, P. Debris microscopiques d'eurypterides du Paleozoique saharien. *Revue de Micropaleontologie*, **1967**, 10, 119-127, pl. 1, 2.
41. Miller, M.A. Chapter 13E. Invertebrate cuticular fragments; in: Jansonius, J. and McGregor, D.C. (ed.), Palynology: principles and applications. *American Association of Stratigraphic Palynologists Foundation*, **1966**, 1, p. 381-382.
42. Braun, A. Occurrence, investigation methods and significance of animal cuticle in Devonian and Carboniferous coal-bearing sedimentary rocks. *Palaeontographica Abteilung* **1997**, A 245, 83–156.
43. Makled A.W.; Al-Auqadi, R.S.; Al-Juboury, A.I.; El Garhy, M.M.; Alarifi, N.; Omar, N.; Mahmoud, A. (2024). Eurypterid setae and cuticle fragments from the Ora Fomation (Upper Devonian) of Iraq. *Palynology*. https://doi.org/10.1080/01916122.2024.2445034
44. Mikrotax [Woodside Energy and Shell USA]. (2024). Ascidian spicules [Nannotax3 website]. Retrieved from https://www.mikrotax.org/Nannotax3/index.php?taxon=Ascidian%20spiculesandmodule=non_cocco
45. Flügel, E.A. *Microfacies of carbonate rocks: analysis, interpretation and application*, **2010**, *976*, p. 2004. Berlin, Springer.
46. Katz, B.J. Controlling factors on source rock development—a review of productivity, preservation, and sedimentation rate. In: Harris, N. (Ed). Deposition of Organic-Carbon-Rich Sediments: Models, Mechanisms, and Consequences, SEPM Special Publication 82, **2005**, 7–16.
47. Röhl, H.-J.; Schmid-Röhl, A. Lower Toarcian (Upper Liassic) Black Shales of the Central European Epicontinental Basin: A Sequence Stratigraphic Case Study from the SW German Posidonia Shale. In:

 doi:10.20944/preprints202603.1900.v1

Harris, N. (Ed). Deposition of Organic-Carbon-Rich Sediments: Models, Mechanisms, and Consequences, SEPM Special Publication 82, **2005**, 165–189.

48. Abou El-Anwar, E.; Salman, S.; Makled, W.; Mousa, D.; Gentzis, T., Shazly, T.F. Depositional mechanism of Duwi Formation organic-rich rocks in anoxic Campanian-early Maastrichtian condensed sections in the Qusseir–Safaga region in Eastern Desert of Egypt and their economic importance. *Marine and Petroleum Geology*, **2024**, *163*, 106759.
49. Van Wagoner, J.C.; Mitchum, R.M.; Campion, K.M.; Rahmanian, V.D. Siliciclastic sequence stratigraphy in well logs, cores, and outcrops: concepts for high-resolution correlation of time and facies. *American Association of Petroleum Geologists*, **1990**, *7*. DOI: https://doi.org/10.1306/Mth7510
50. Gao, P.; Khong, H.Y.; Wibowo, A.; Zhen, Y.; Peng, C.; Miao, W. Chemical compositions and nutritional profiles of two edible tunicate species (Halocynthia roretzi and Halocynthia aurantium). *Heliyon*, **2024**, *10*(12).
51. Millar, R.H. The biology of ascidians. In *Advances in Marine Biology*, **1971**, *9*, p. 1-100, Academic Press.
52. O'Brien, G.W.; Milnes, A.R.; Veeh, H.H.; Heggie, D.T.; Riggs, S.R.; Cullen, D.J.; Marshall, J.F.; Cook, P.J. Sedimentation dynamics and redox iron-cycling: controlling factors for the apatite-glauconite association on the East Australian continental margin. In: Northolt, A.J.G., Jarvis, I. (Eds.), Phosphorite Research and Development, vol. 52. Geological Society of London Special Publication, **1990**, pp. 61–86.
53. Scholle, P.A.; Ulmer-Scholle, D.S. *A color guide to the petrography of carbonate rocks: grains, textures, porosity, diagenesis, AAPG Memoir 77*, **2003**, 77.
54. Tang, D.; Xie, B.; Shi, X.; Zhou, X. Low level of phosphorous concentration in terminal Paleoproterozoic shallow seawater: Evidence from Chuanlinggou ironstone on North China Platform. *Precambrian Research*, **2022**, 370, 106554.
55. Rudmin, M.; Mazurov, A.; Banerjee, S. Origin of ooidal ironstones in relation to warming events: Cretaceous-Eocene Bakchar deposit, south-east Western Siberia. *Marine and Petroleum Geology*, **2019**, *100*, 309-325.
56. Abram, M.B.; Holz, M. Early to Middle Devonian ironstone and phosphorite in the northwestern Gondwana Parnaíba Basin, Brazil: A record of an epeiric margin paleoceanographic changes. *Sedimentary Geology*, **2020**, *402*, 105646.
57. Rudmin, M.; Banerjee, S.; Maximov, P.; Novoselov, A.; Trubin, Y.; Smirnov, P.; ... and Mazurov, A. Origin of ooids, peloids and micro-oncoids of marine ironstone deposits in Western Siberia (Russia). *Journal of Asian Earth Sciences*, **2022**, *237*, 105361.
58. Vodrážková, S.; Kumpan, T.; Vodrážka, R.; Frýda, J.; Čopjaková, R.; Koubová, M.; ... and Holá, M. Ferruginous coated grains of microbial origin from the Lower Devonian (Pragian) of the Prague Basin (Czech Republic)–Petrological and geochemical perspective. *Sedimentary Geology*, **2022**, *438*, 106194.
59. Zhou, M.F.; Lyu, Y.J.; Liu, Z.R.; Liu, P.P.; Meng, L.; Qiu, W.J.; Zhao, W.W. Devonian stratiform ironstone deposits in South China formed in a shallow marine environment of a passive continental margin. *Journal of Asian Earth Sciences*, **2024**, *262*, 105997.
60. Young, T.P. Eustatically controlled ooidal ironstone deposition: facies relationships of the Ordovician open-shelf ironstones of Western Europe. *Geological Society, London, Special Publications*, **1989**, *46*(1), 51-63.
61. Peryt, T.M. Phanerozoic oncoids—an overview. *Facies*, **1981**, *4*, 197–213.
62. Jones, B.; Renaut, R.W. Formation of silica oncoids around geysers and hot springs at El Tatio, Chile. *Sedimentology*, **1997**, *44*, 287–304.
63. Riding, R. Microbial carbonates: the geological record of calcified bacterial–algal mats and biofilms. *Sedimentology*, **2000**, *47*, 179–214.
64. Védrine, S.; Strasser, A.; Hug, W. Oncoid growth and distribution controlled by sea level fluctuations and climate (Late Oxfordian, Swiss Jura Mountains). *Facies*, **2007**, *53*, 535–552.
65. Bádenas, B.; Aurell, M. Facies models of a shallow-water carbonate ramp based on distribution of non-skeletal grains (Kimmeridgian, Spain). *Facies*, **2010**, *56*, 89–110.
66. Zaton, M.; Kremer, B.; Marynowski, L.; Wilson, M.A.; Krawczynski, W. Middle Jurassic (Bathonian) encrusted oncoids from the Polish Jura, southern Poland. *Facies*, **2012**, *58*, 57–77.

 doi:10.20944/preprints202603.1900.v1

67. Sequero, C.; Aurell, M.; Bádenas, B. Sedimentary evolution of a shallow carbonate ramp (Kimmeridgian, NE Spain): unravelling controlling factors for facies heterogeneities at reservoir scale. *Marine and Petroleum Geology*, **2019**, *109*, 145–174.
68. Sequero, C.; Aurell, M.; Bádenas, B. Oncoid distribution in the shallow domains of a Kimmeridgian carbonate ramp (Late Jurassic, NE Spain). *Sedimentary Geology*, **2020**, *398*, 105585.
69. Stasiuk, L.D.; Fowler, M.G. Organic facies in Devonian and Mississippian strata of Western Canada Sedimentary Basin: relation to kerogen type, paleoenvironment, and paleogeography. *Bulletin of Canadian Petroleum Geology*, **2014**, *52*(3), 234–255.
70. Stasiuk, L.D. Microscopic Studies of Sedimentary Organic Matter: Key to Understanding Organic-Rich Strata, with Paleozoic Examples from Western Canada Basin. *Geoscience Canada*, **1999**, *26*(4), 149–172.
71. Loutit, T.S.; Hardenbol, J.; Vail, P.R.; Baum, P. Condensed sections: the key to age determination and correlation of continental margin sequences. In: Wilgus, C.K., Hastings, B.S., Posamentier, H., Van Wagoner, J., Ross, C.A., Kendall, C.G.S.C. (Eds.), Sea-level Changes — An Integrated Approach. Society of Economic Paleontologists and Mineralogists, Special Publication 42, **1988**, pp. 183–213.
72. Föllmi, K.B. Sedimentary condensation. *Earth-Science Reviews*, **2016**, *152*, 143-180
73. Hallett, D.; Clark-Lowes, D. *Petroleum geology of Libya*. *Elsevier*. **2017**, p. 391.
74. Rubino, J.L.; Blanpied, C. Sedimentology and sequence stratigraphy of the Devonian to lowermost Carboniferous succession on the Gargaf Uplift (Murzuq Basin, Libya). In *Geological Exploration in Murzuq Basin*, **2000**, 321-348, Elsevier Science BV.
75. Guerrak, S. Time and space distribution of Palaeozoic oolitic ironstones in the Tindouf Basin, Algerian Sahara. *Geological Society, London, Special Publications*, **1989**, *46*(1), 197-212.